

**NASA CONTRACTOR
REPORT**

NASA CR-1929



NASA CR
C.1

0060988



TECH LIBRARY KAFB, NM

LOAN COPY: RETURN TO
AFWL (DOLL)
KIRTLAND AFB, N. M.

**ISOTHERMAL ELASTOHYDRODYNAMIC
THEORY FOR THE FULL RANGE
OF PRESSURE-VISCOSITY COEFFICIENT**

by H. S. Cheng

Prepared by
NORTHWESTERN UNIVERSITY
Evanston, Ill.
for Lewis Research Center

NATIONAL AERONAUTICS AND SPACE ADMINISTRATION • WASHINGTON, D. C. • SEPTEMBER 1971



0060988

1. Report No. NASA CR-1929		2. Government Accession No.		3. Recipient's Catalog No.	
4. Title and Subtitle ISOTHERMAL ELASTOHYDRODYNAMIC THEORY FOR THE FULL RANGE OF PRESSURE-VISCOSITY COEFFICIENT				5. Report Date September 1971	
				6. Performing Organization Code	
7. Author(s) H. S. Cheng				8. Performing Organization Report No. None	
				10. Work Unit No.	
9. Performing Organization Name and Address Northwestern University Evanston, Illinois				11. Contract or Grant No. NGL 14-007-084	
				13. Type of Report and Period Covered Contractor Report	
12. Sponsoring Agency Name and Address National Aeronautics and Space Administration Washington, D. C. 20546				14. Sponsoring Agency Code	
15. Supplementary Notes Project Manager, Erwin V. Zaretsky, Fluid System Components Division, NASA Lewis Research Center, Cleveland, Ohio					
16. Abstract <p>The isothermal, elastohydrodynamic (EHD) solutions for line contacts are extended to cover the full range of pressure-viscosity parameter, G, and the region of extremely heavy loads. The effect of a composite exponential model for the pressure-viscosity dependence on the film thickness is also studied. Results of the film thickness are compared with those based on work by Grubin, Dowson-Higginson, Bell and Kannel, and Herrebrugh. Comparison is also made between the theoretical results and the recently obtained X-ray film thickness measurements.</p>					
17. Key Words (Suggested by Author(s)) Elastohydrodynamics Lubrication Rheology Rolling bearings				18. Distribution Statement Unclassified - unlimited	
19. Security Classif. (of this report) Unclassified		20. Security Classif. (of this page) Unclassified		21. No. of Pages 53	22. Price* \$3.00

CONTENTS

	Page
I. INTRODUCTION	1
II. SUMMARY OF EHD FILM THICKNESS FORMULATION	3
III. GOVERNING EQUATIONS	3
IV. DISCUSSION OF RESULTS	4
A. Inlet Solutions For Oils With A Constant Pressure-Viscosity Coefficient	5
B. Inlet Solutions For Oils With Composite Pressure-Viscosity Coefficients	6
C. Typical Outlet Solution	7
V. COMPARISON WITH EXPERIMENTS AND OTHER THEORIES	7
A. Thermal Reduction Factor	8
B. Comparison of Results	9
VI. CONCLUSIONS	12
REFERENCES	14
TABLES	16
APPENDIXES	
A - NOMENCLATURE	19
B - NUMERICAL SOLUTION FOR THE INLET REGION	22
FIGURES	27

I. INTRODUCTION

Because of the strong influence of elastohydrodynamic (EHD) lubrication upon the failures of heavily loaded rolling contacts, the EHD problem has received considerable attention in the past decade. Comprehensive review of the progress on EHD up to 1965 was made by Dowson [1] and Archard [2] and more recently was covered by McGrew et al [3].

For the most part, the emphasis of EHD, is still on the film thickness level and the film thickness distribution within the contact. On the analytical side, there have been film thickness formulae developed by Grubin [4], Dowson and Higginson [5], Archard and Cowking [6] and Crook [7], and Cheng [8]. Within the range of moderate speeds and loads (below 500 in/sec (12.7 m/sec) and 100,000 psi ($6.89 \times 10^8 \text{ N/m}^2$) max. Hertz stress for steel contacts), and within a limited range of pressure-viscosity coefficients, these film thickness theories have been shown to agree reasonably well with the measured film thickness by Crook [9], Sibley and Orcutt [10], Christensen [11], and Dyson, Naylor, and Wilson [12]. The good agreement between the above theories and experiments has led to a wide acceptance of using Dowson-Higginson type of formulae to predict EHD film thicknesses.

For high load and high speed cases, the prediction of film thickness by using Grubin or Dowson-Higginson formula is grossly inadequate. This fact has been demonstrated by the film thickness measurement by

Kannel et al [13] using the X-ray technique. The X-ray data has consistently shown that the dependence of the minimum film thickness upon load under heavy loads is far higher than that appeared in the Dowson-Higginson theory.

Several explanations have been suggested as the possible cause for discrepancy between the measured film data and those calculated by the isothermal theory. These are: 1) the heating effect at the inlet region, 2) the inability of the viscosity to arise with pressure according to the static pressure-viscosity experiment during a short time interval, and 3) loss of viscosity due to high-shear rate at high speeds.

The inclusion of heating effects in the Grubin-type inlet analysis has been examined thoroughly in a recent report by Cheng [14]. The thermal analysis can account for a major part of the loss of film generating capacity at high speeds, but it fails to show the high load-dependence as observed in X-ray data. Consequently, further work is needed in determining the effect of a reduced pressure-viscosity coefficient and the effect of a shear-rate-dependent viscosity upon the EHD film thickness formation.

The effect of reduced pressure-viscosity coefficient cannot be examined by the existing Grubin or Dowson-Higginson formula, since in both formulae the assumption of a high pressure-viscosity coefficient is required. To develop film thickness data valid for conditions approaching isoviscous cases, it is necessary to extend the full EHD solution to regions of high loads and low pressure-viscosity coefficients. Such has been the major objective of this research.

II. SUMMARY OF EHD FILM THICKNESS FORMULATION

It is well known that the ratio of the EHL film thickness to the effective radius is governed by three non-dimensional parameters, the speed, load, and pressure-viscosity coefficient parameters. A survey of all EHL film thickness formulae shows that both the nominal film thickness, h_o , or the minimum film thickness h_{\min} , in a line or point elastohydrodynamic contact can be put into the following general expression:

$$\frac{h}{R} = C G^{n_1} \bar{U}^{n_2} \bar{P}_{hz}^{n_3} \quad (1)$$

where C is a constant and n_1 , n_2 , and n_3 are the exponents for the non-dimensional lubricant, speed, and load parameters respectively. The distinction between nominal and minimum film thickness is shown in Fig. 1. Values of C , n_1 , n_2 and n_3 based on analyses by Grubin [4], Dowson and Higginson [5], Crook [7], Archard and Cowking [6], and Cheng [8], are listed in Table 1. It is seen that the agreement among various theories is very good with regard to load or speed dependence.

III. GOVERNING EQUATIONS

Referring to [15], the two coupled equations governing the pressure and film distributions in an elastohydrodynamic line contact between two rollers (Fig. 2) are:

1. The Reynolds Equation

$$\frac{dp}{dx} = 6\mu(u_1 + u_2) \left(\frac{h - h^* \frac{\rho}{\rho^*}}{h^3} \right) \quad (2)$$

2. The Elasticity Equation

$$h = h^* + \frac{x^2 - x^{*2}}{2R} - \frac{4}{\pi E'} \int_{-\infty}^{x_f} \ln \frac{|\xi - x|}{|\xi - x^*|} p(\xi) d\xi \quad (3)$$

In non-dimensional form, these equations become

$$\frac{dP}{d\bar{x}} = \left(\frac{48}{H^{*2}} \right) \bar{U} \bar{\mu} \left(\frac{H - \bar{\rho} / \bar{\rho}}{H^3} \right) \quad (4)$$

$$H = 1 + \frac{16 \bar{P}_{hz}^2}{H^{*2}} \left(\frac{\bar{x}^2}{2} - \frac{1}{\pi} \int_{-\infty}^{\bar{x}_f} P(\bar{\xi}) \ln \frac{|\bar{\xi} - \bar{x}|}{|\bar{\xi} - \bar{x}^*|} d\bar{\xi} \right) \quad (5)$$

where the non-dimensional variables are defined in the Nomenclature.

Since the primary interest in this investigation is to extend the present EHD solutions to extremely heavily loaded regions, the pressure distribution in nearly all of the contact region would coincide with the Hertzian elliptical profile. Taking advantage of this fact, one may divide the problem in two parts, the inlet and the exit solutions. The inlet solution determines the film thickness level in the conjunction, and the exit solution furnishes the details of the protrusion before the film terminates.

Numerical solutions for the inlet as well as the exit region differ slightly with that presented earlier [15] in order to make provisions for viscosities varying arbitrarily with pressure. The numerical procedures for the inlet analysis are documented in the Appendix.

IV. DISCUSSION OF RESULTS

Considerable data have been obtained for a lubricant having a constant pressure-viscosity coefficient. These data cover a wide range of pressure-viscosity coefficients from a nearly isoviscous lubricant, $\alpha \rightarrow 0$, to $\alpha = 10^{-4}$ in²/lb (1.45 x 10⁻⁸ m²/N), which is comparable to the coefficients for mineral oils. The load range has been extended to

maximum Hertz pressures equal to 4×10^5 psi (2.76×10^9 N/m²) for steel contacts. Some typical runs were also made for lubricants with a composite pressure-viscosity coefficients, and for the pressure and deformation profiles in the exit region.

A. Inlet Solutions for Oils with a Constant Pressure-Viscosity Coefficient

Results in this section were obtained for the most commonly used viscosity model for which the viscosity varies exponentially with the pressure.

$$\mu = \mu_0 e^{\alpha p} \quad (6)$$

For this model, data were generated for the speed parameter, \bar{U} , from 10^{-13} to 10^{-8} , for the load parameter, \bar{P}_{hz} , from 0.003 to 0.012, and for the pressure-viscosity parameter, G , from 50 to 3000. These results are tabulated in Table 2.

The effect of the speed parameter on the dimensionless center film thickness, H_c , is shown in Figs. 3a through 3e for various \bar{P}_{hz} and G . The straight line relationship between H_c and \bar{U} holds true over a wide range of \bar{U} for all cases. However, the slope of these curves varies slightly with respect to the pressure-viscosity parameter G as well as the load parameter. The exponent for \bar{U} in the power relation,

$$H_c = C \bar{U}^{n_2} \quad (7)$$

is 0.625 for the case of $G \rightarrow 0$. This value agrees well with the isoviscous theory provided by Herrebrugh [16]. At higher values of G , the exponent n_2 is found to be 0.69 and 0.725 for \bar{P}_{hz} equal to 0.003 and 0.012 respectively. These values seem to agree well with that appeared in the Dowson-Higginson's formula.

The effect of load on H_c can be seen in Figs. 4a through 4e in which H_c is plotted against \bar{P}_{hz} with \bar{U} and G as parameters. The load dependence is measured by the slope of these logarithmic plots. The load exponent n_3 varies slightly with respect to G , but is practically unaffected by \bar{U} . For $G \rightarrow 0$, n_3 is equal to -0.5 which again agrees very well with Herrebrugh's isoviscous solution; for $G = 3000$, n_3 is reduced to -0.36 which is slightly higher than that given in Dowson-Higginson formula.

Unlike the influence of load or speed on H_c , the dependence of film thickness upon the pressure-viscosity coefficient is not linear on the log-log plot. This is demonstrated in Fig. 5 by plotting the variation of H_c with G . For high values of G , the power relationship prevails and the exponent for G in this region is found to be approximately 0.6, which confirms the Dowson-Higginson theory.

For small value of G , the curves become flat, and H_c becomes independent of G and approaches to the isoviscous value provided by Herrebrugh. Fig. 6 gives another representation of these results in terms of the parameters proposed by Moes [17]. In this plot, the number of non-dimensional parameter is reduced by one. One can also obtain similar plots in terms of the three parameters proposed recently by Greenwood [18].

B. Inlet Solutions for Oils with Composite Pressure-Viscosity Coefficients

A few computer runs were also made for oils for which the relation between $\ln \mu$ and p is represented by two straight lines with a steeper line at low pressures and a flatter line at high pressures. This is known as the composite exponential model, which was first introduced by Allen, Townsend, and Zaretsky [19] in the study of spin friction in elliptical contacts.

Fig. 7 shows the viscosity and pressure relationship for the composite exponential model suggested in [19]. The discontinuity in slope at the cut-off pressure has been smoothed out in order to avoid any possible numerical difficulties introduced by this abrupt change in slope. Typical results using this method are shown in Table 3. It is seen that the difference between the straight exponential model and the composite exponential model is insignificantly small. These numerical results definitely support the argument put forth recently by Bell and Kannel [21]. Using a simple Grubin type analysis he showed that the inlet film thickness is largely governed by the pressure-viscosity effect in the low pressure region. Unless the cut-off pressure in the composite exponential model is very small, otherwise the reduction of the pressure-viscosity dependence at high pressures introduced by the composite model has very little influence upon the film thickness.

C. Typical Outlet Solution

Results in the outlet section show no significantly different results from the previous EHD solutions. Figure 8 shows typical pressure and film profiles for $\bar{P}_{hz} = 0.003$, $G = 3000$, and $H_c = 10^{-5}$. The minimum film thickness is approximately 80% of the center film thickness and 70% of the inlet film thickness.

V. COMPARISON WITH EXPERIMENTS AND OTHER THEORIES

The experimental data which are selected to compare with the present analytical data are those obtained recently by the X-ray technique in Ref. 20.

Figs. 9a to 9e show a plot of the measured minimum film thickness against the maximum Hertz stress for various rolling speeds and ambient temperature. These were obtained with a pair of

crowned-cone disks; the lubricant is a synthetic paraffinic hydrocarbons with no additives.

Since the rolling speeds for these tests are in the range where the heating has a significant influence on the film-forming capability, direct correlations between the present analytical data and the X-ray data will not be meaningful unless some corrections for thermal effects are made on the analytical data. Such corrections were achieved by using the thermal reduction factors provided by Cheng [14].

A. Thermal Reduction Factor

In Ref. [14], it was shown that the thermal reduction factor, ϕ_T defined as the ratio of the actual film thickness to the isothermal film thickness based on the Dowson-Higginson formula, is a function of the following five parameters:

$$Q_m = \frac{\mu_o (u_2 + u_1)^2}{2K_f T_o} = \text{heating parameter}$$

$$G = \alpha E' = \text{non-dimensional pressure-viscosity coefficient}$$

$$\beta' = \frac{\beta}{T_o} = \text{non-dimensional temperature-viscosity coefficient}$$

$$\bar{P}_{hz} = \frac{P_{hz}}{E'} = \text{load parameter}$$

$$S = \frac{u_1 - u_2}{u_1} = \text{slip}$$

These thermal reduction factors are obtained by solving the coupled energy and Reynold equation at the inlet region using the Hertzian deformation profile. The heat convected by the lubricant and the heat conducted by

the disc are both considered.

The lubricant properties for this synthetic paraffinic oil for an ambient temperature of 150°F (338.5°K) are estimated as

$$\begin{aligned} \mu_o &= \text{inlet viscosity} = 1.45 \times 10^{-5} \text{ lb-sec/in}^2 \text{ (0.1 N-sec/m}^2\text{)} \\ \alpha &= \text{pressure-viscosity coefficient} = 1.5 \times 10^{-4} \text{ in}^2/\text{lb} \text{ (} 2.18 \times 10^{-8} \text{ m}^2/\text{N} \text{)} \\ \beta &= \text{Temperature-viscosity coefficient} = 7700 \text{ }^\circ\text{R (4280 }^\circ\text{K)} \\ \gamma &= \text{pressure-temperature-viscosity coefficient} = 0.145 \text{ }^\circ\text{R-in}^2/\text{lb} \text{ (} 1.17 \times 10^{-5} \text{ }^\circ\text{K - m}^2/\text{N)} \\ K_f &= \text{thermal conductivity of the lubricant} = 0.0216 \text{ lb/sec-}^\circ\text{R (0.1725 N/sec-}^\circ\text{K)} \end{aligned}$$

Fig. 10 shows the variation of the thermal reduction factor with the heating parameter Q_m corresponding to the lubricant properties for this sythetic paraffinic oil. Using this curve, the values of ϕ_T for the ambient temperatures of 150 and 300°F (338.5 and 421.5°K), and the rolling speeds of 5000 and 20,000 RPM are given as below

	$T_o = 150^\circ\text{F (338.5}^\circ\text{K)}$		$T = 300^\circ\text{ (421.5}^\circ\text{K)}$	
	N=5000 RPM	N=20,000 RPM	N=5000 RPM	N=20,000 RPM
Q_m	0.31	4.94	.0373	0.596
ϕ_T	0.76	0.31	0.92	0.67

B. Comparison of Results

The present analytical results are compared with experimental X-Ray data [20]

at $T_o = 150$ and 300°F and $N = 5000$ and $20,000$ RPM in Figs. 11a through 11e. Along with the experimental data, the calculated film thickness based on earlier EHD theories by Grubin [3], Dowson and Higginson [4], and based on more recent isoviscous formulae by Herrebrugh [16], and Bell and Kannel [21].

In these figures, the minimum film thicknesses are plotted against the maximum Hertzian pressure. In calculating the Grubin's film thickness, a reduction factor 0.75 has been used in order to convert the nominal film to minimum film thickness. For the data in the present analysis, a factor of 0.8 has been used in converting the center film thickness to the minimum film thickness. For Grubin, Bell and Herrebrugh's work, the results are given in terms of minimum film thickness; therefore, no reductions are required. Figure 11 shows the comparison of the experimental results with all theories without any corrections for thermal effects, $\phi_T = 1$. It is seen that the measured data come very close to the isoviscous data by Herrebrugh indicating that all the pressure-viscosity effects may have been lost due to the combined thermal and non-Newtonian effects.

Among the isothermal theoretical data, the Grubin or Dowson-Higginson formulae (based on $G_o = 4950$ at 150°F) predict minimum films almost one order of magnitude higher than the isoviscous data. In the range of high G , the present theory agrees closely with D-H data. In the extremely low G range where the lubricant is practically isoviscous, this theory shows a complete overlap with Herrebrugh's isoviscous data. The recent theory by Bell and Kannel [21] based on a time-delayed pressure-viscosity model predicts a load dependence much stronger than all other EHD theories. Since this trend is much closer to that observed at higher loads, it is

very tempting to believe their approximate inlet analysis using the time-delayed pressure-viscosity model. However, a closer examination of their conclusion that the dependence of film thickness upon 10/11th power of maximum Hertzian stress is a consequence of the application of Grubin's method for an isoviscous lubricant ($\alpha \rightarrow 0$). While the Grubin's approach yields an accurate solution for lubricant with high α , it is grossly inadequate for isoviscous fluids. This is further evidenced by the lack of agreement between the Grubin's load exponent for the isoviscous case (10/11) and the Herrebrugh's load exponent (1/2) which is obtained from a complete EHD analysis. Thus, the strong load dependence found in Bell and Kennel's theory may be a direct consequence of the Grubin-type approximation rather than a result from the use of time-delayed, pressure-viscosity model.

Figure 11b shows the same comparison as in Fig. 11a except with φ_T included in all the calculated film thickness. By accounting for thermal effects, the experimental data agrees reasonably well in the low-load region with the present theory for $G = 3000$, particularly in trends. For high loads, there seems to be a drastic reduction in film thickness as the load increases. This sudden increase in load dependence appears to be caused by the loss of pressure-viscosity dependence at high loads.

The comparison for three other operating conditions is shown in Fig. 11c through 11e. The general features of these curves are in same as those in Fig. 11b except the level changes slightly. For $N = 5000$ RPM and 150°F , the experimental thickness in the low-load range approaches an equivalent pressure-viscosity coefficient of 2000 which is slightly lower than the value for 20,000 RPM. For the cases of the higher ambient temperature, further reduction of the pressure-viscosity

effects are evidenced.

Figure 12 plots the intercepts between the experimental curve and the curves for various values of G calculated from the present theory. These are interpreted as the variation of the effective pressure-viscosity coefficient with the increase of load. The drastic reduction of pressure-viscosity dependence at high pressures is clearly seen in these curves.

VI. CONCLUSIONS

1. The extensions of isothermal EHD results in the extremely heavily loaded region and in the region of moderate and low pressure-viscosity dependence show that:
 - a) The dependence of film thickness on load in the region of heavy loads and low pressure-viscosity dependence is slightly stronger than that predicted by the previous isothermal EHD theories. The load exponent in the film thickness formula, Eq. (1), is -0.5 instead of -0.26 given in Dowson-Higginson formula [5].
 - b) The power relationship between the film thickness and the pressure-viscosity parameter, G , only holds at high values of G . As G decreases, the dependence of film thickness on G becomes steadily weaker. For $G \rightarrow 0$, the film thickness is independent of G as predicted by Herrebrugh [16].
2. The loss of pressure-viscosity dependence in the high pressure region, as illustrated by the composite exponential model [19], has a negligible effect on the film-forming capability in the inlet of an EHD contact.
3. Comparison between the calculated minimum film with the present theory and the recent measured, X-Ray data for a synthetic paraffinic, lubricant, shows that:

- a) In the moderately loaded regime, there is little dispute between EHD theories and the measured data. They agree well both in trends and in magnitude.
- b) In the extremely heavily loaded regime, the measured film shows a drastic reduction of film with respect to the load, and this sharp reduction does not appear to be predictable by the present isothermal EHD theories.

References

1. Dowson, D., "Elastohydrodynamic Lubrication: An Introduction and Review of Theoretical Studies," Lubrication and Wear Group Symposium on EHL, Paper R1.
2. Archard, J. F., "Experimental Studies of Elastohydrodynamic Lubrication," Lubrication and Wear Group Symposium on EHL, Paper R2.
3. McGrew, J., Gu, A., Cheng, H. S., and Murray, F., "Elastohydrodynamic Lubrication, Phase I," Technical Documentary Report ASD-TDR-Phase I.
4. Grubin, A. N. and Vinogradova, I. E., Central Scientific Research Institute for Technology and Mechanical Engineering, Book No. 30 (Moscow): D.S.I.R. Trans. No. 337.
5. Dowson, D. and Higginson, G. R., "The Effect Of Material Properties On the Lubrication of Elastic Rollers," J. Mech. Engng. Sci. 2(3), 188.
6. Archard, J. F. and Cowking, E. W., "A Simplified Treatment of Elastohydrodynamic Lubrication Theory for a Point Contact," Lubrication and Wear Group Symposium on Elastohydrodynamic Lubrication Paper 3 (Instn Mech. Engrs., London).
7. Crook, A. W., "The Lubrication Of Rollers - II. Film Thickness With Relation to Viscosity And Speed," Phil. Trans. Series A 254, 223.
8. Cheng, H. S., "A Numerical Solution of the Elastohydrodynamic Film Thickness in an Elliptical Contact," Journal of Lubrication Technology, Trans. of ASME, Vol. 92, Series F. No. 1, Jan. 1970.
9. Crook, A. W., "The Lubrication of Rollers - I," Phil. Trans. Series A 250, 387.
10. Sibley, L. B. and Orcutt, F. K., "Elastohydrodynamic Lubrication of Rolling Contact Surfaces," Amer. Soc. Lubric. Engrs. 4 (2), 234.
11. Christensen, H., "The Lubrication of Rolling Contacts, Measurement of Film Thickness," Acta Polytech Scand. Mech. Engng Series 15.
12. Dyson, A., Naylor, H. and Wilson, A. R., "The Measurement of An Oil Film Thickness in Elastohydrodynamic Contacts," Lubrication and Wear Group Symposium on Elastohydrodynamic Lubrication, Paper 10 (Instn Mech. Engrs., London).
13. Kannel, J. W., et. al., "A Study of the Influence of Lubricants on High-Speed Rolling-Contact Bearing Performance," ASD TECH. Rep. No. ASD-TDR-61-643, Part VIII (June, 1968).

14. Cheng, H. S., (1967), "Calculations of Elastohydrodynamic Film Thickness in High Speed Rolling and Sliding Contacts," Mechanical Technology, Inc. Technical Report, MTI-67TR24.
15. Cheng, H. S. and Sternlicht, B. (1965), "A Numerical Solution for Pressure, Temperature, and Film Thickness Between Two Infinitely Long Rolling and Sliding Cylinders Under Heavy Load," Journal of Basic Engineering, Trans. of ASME, Series D, Vol. 87, No. 3, 1965, pp. 695-707.
16. Herrebrugh, K. (1968), "Solving the Incompressible and Isothermal Problem in Elastohydrodynamic Lubrication Through an Integral Equation," Journal of Lubrication Technology, Trans. of ASME, Vol. 90, Series F., No. 1, Jan. 1968, pp. 262-270.
17. Moes, H., Jr., (1965), "Communications to EHL Symposium held at Leeds University, 1965," Proc. Institute Mech. Engrs. Vol. 180, Pt 3B, pp. 244.
18. Greenwood, J., (1970), "A Re-Examination of EHL Film-Thickness Measurements," Wear, Vol. 15, 1970, pp. 281-289.
19. Allen, C. W., Townsend, D., and Zaretsky, (1970), "Elastohydrodynamic Lubrication of a Spinning Ball in a Nonconforming Groove," Journal ASME, Series F, Vol. 92, No. 1, Jan. 1970, pp. 89-96.
20. Parker, R. J. and Kannel, J. W., "Elastohydrodynamic Film Thickness Between Rolling Disks with a Synthetic Paraffinic Oil to 600^oF," NASA TN in Process, 1971.
21. Bell, J. C. and Kannel, J. W., (1971), "Interpretations of the Thickness of Lubricant Films in Rolling Contact II - influence of Possible Rheological Factors," ASME Paper No. 71-LUB-T, 1971, to appear in Journal of Lubrication Technology.
22. Wernick, R. J., (1963), "Some Computer Results in the Direct Iteration Solution of the Elastohydrodynamic Equations," Mech. Tech. Inc. Tech. Report MTI-62-TR-38.

TABLE 1 CONSTANTS AND COEFFICIENTS FOR
EHD FILM THICKNESS FORMULAE

$$\frac{h}{R} = C G^{n_1} \bar{U}^{n_2} \bar{P}_{hz}^{n_3}$$

CONTRIBUTOR	C	n ₁	n ₂	n ₃	REMARK
GRUBIN	1.65	0.73	0.73	- .18	FOR NOMINAL FILM, h _o , $\frac{a}{b} = \infty$
CROOK	1.68	-.75	0.75	- .25	FOR NOMINAL FILM, h _o , $\frac{a}{b} = \infty$
DOWSON & HIGGINSON	1.26	0.6	0.7	- 0.26	FOR MINIMUM FILM, h _{min} , $\frac{a}{b} = \infty$
ARCHARD	1.37	0.74	0.74	- 0.22	FOR NOMINAL FILM, h _o , AND POINT CONTACT, a/b = 1.0
CHENG	1.625	0.74	0.74	- 0.22	FOR NOMINAL FILM, h _o , $\frac{a}{b} \geq 5.0$
	1.56	0.736	0.736	- 0.209	FOR NOMINAL FILM, h _o , $\frac{a}{b} = 2.0$
	1.415	0.725	0.725	- 0.174	FOR NOMINAL FILM, h _o , $\frac{a}{b} = 1.0$
	1.22	0.688	0.688	- .066	FOR NOMINAL FILM, h _o , $\frac{a}{b} = 0.5$

$\frac{a}{b}$ = ratio of semi-major to semi-minor axis of the contact ellipse (a/b → ∞ line contact)

TABLE 2. ISOTHERMAL EHL FILM THICKNESS FOR FULL RANGE OF
 PRESSURE VISCOSITY COEFFICIENTS, H_c vs. \bar{U} WITH \bar{P}_{hz} AND G
 AS PARAMETERS.

G	H_c	$\bar{P}_{hz} = .003$	$\bar{P}_{hz} = .006$	$\bar{P}_{hz} = .009$	$\bar{P}_{hz} = .012$
		\bar{U}	\bar{U}	\bar{U}	\bar{U}
50	1×10^{-5}	1.9069×10^{-11}	3.3718×10^{-11}	4.6116×10^{-11}	5.7839×10^{-11}
	5×10^{-6}	6.3775×10^{-12}	1.1304×10^{-11}	1.5589×10^{-11}	1.9437×10^{-11}
	2×10^{-6}	1.4737×10^{-12}	2.6158×10^{-12}	3.6388×10^{-12}	4.5094×10^{-12}
	1×10^{-6}	4.8547×10^{-13}	8.3793×10^{-13}	1.1864×10^{-12}	1.46607×10^{-12}
500	1×10^{-5}	1.332×10^{-11}	2.127×10^{-11}	2.766×10^{-11}	3.304×10^{-11}
	5×10^{-6}	4.616×10^{-12}	7.510×10^{-12}	9.853×10^{-12}	1.183×10^{-11}
	2×10^{-6}	1.129×10^{-12}	1.870×10^{-12}	2.472×10^{-12}	2.998×10^{-12}
	1×10^{-6}	3.851×10^{-13}	6.452×10^{-13}	8.597×10^{-13}	1.062×10^{-12}
1000	1×10^{-5}	9.980×10^{-12}	1.519×10^{-11}	1.973×10^{-11}	2.273×10^{-11}
	5×10^{-6}	3.548×10^{-12}	5.521×10^{-12}	7.085×10^{-12}	8.381×10^{-12}
	2×10^{-6}	8.979×10^{-13}	1.430×10^{-12}	1.851×10^{-12}	2.231×10^{-12}
	1×10^{-6}	3.142×10^{-13}	5.104×10^{-13}	6.665×10^{-13}	8.287×10^{-13}
2000	1×10^{-5}	6.661×10^{-12}	9.724×10^{-12}	1.211×10^{-11}	1.408×10^{-11}
	5×10^{-6}	2.434×10^{-12}	3.632×10^{-12}	4.562×10^{-12}	5.351×10^{-12}
	2×10^{-6}	6.392×10^{-13}	9.789×10^{-13}	1.247×10^{-12}	1.500×10^{-12}
	1×10^{-6}	2.308×10^{-13}	3.613×10^{-13}	4.689×10^{-13}	5.770×10^{-13}
3000	1×10^{-5}	5.060×10^{-12}	7.19×10^{-12}	8.89×10^{-12}	1.02×10^{-11}
	5×10^{-6}	1.890×10^{-12}	2.70×10^{-12}	3.39×10^{-12}	3.94×10^{-12}
	2×10^{-6}	4.940×10^{-13}	7.43×10^{-13}	9.48×10^{-13}	1.14×10^{-12}
	1×10^{-6}	1.80×10^{-13}	2.79×10^{-13}	3.65×10^{-13}	4.33×10^{-13}

TABLE 3. COMPARISON OF EHL FILM BETWEEN THE STRAIGHT EXPONENTIAL MODEL AND THE COMPOSITE EXPONENTIAL MODEL.

\bar{P}_{hz}	\bar{h}_c	STRAIGHT MODEL	COMPOSITE MODEL
		\bar{U}	\bar{U}
0.003	1×10^{-5}	5.060×10^{-12}	5.012×10^{-12}
	5×10^{-6}	1.890×10^{-12}	1.876×10^{-12}
	2×10^{-6}	4.940×10^{-13}	4.986×10^{-13}
	1×10^{-6}	1.800×10^{-13}	1.831×10^{-13}
0.012	1×10^{-5}	1.020×10^{-11}	1.022×10^{-11}
	5×10^{-6}	3.940×10^{-12}	3.962×10^{-12}
	2×10^{-6}	1.140×10^{-12}	1.135×10^{-12}
	1×10^{-6}	4.330×10^{-13}	4.295×10^{-12}

For straight model $\alpha E = 3000$

For composite model $\alpha_1 E = 3000$

$\alpha_2 E' = 240$

Cut off pressure $\approx 55,000$ psi (2.03×10^6 N/m²)

APPENDIX A - NOMENCLATURE

a	=	semi-major axis of an elliptical contact,	in (m)
A	=	see Eq. (A-18)	
b	=	semi-minor axis of an elliptical contact,	in (m)
B	=	see Eq. (A-18)	
C	=	constant used in the film thickness formula	
C_1	=	$16 \bar{P}_{hz}^2 / H^*$	
C_5	=	$48 \bar{U} / (H^*)^2$	
$1/E'$	=	$\frac{1}{2} \left(\frac{1 - \nu_1^2}{E_1} + \frac{1 - \nu_2^2}{E_2} \right)$	$\text{in}^2 / \text{lb} \left(\frac{\text{m}^2}{\text{N}} \right)$
E_1, E_2	=	Young's Modulus for rollers 1 and 2	$\text{lb} / \text{in}^2 \left(\frac{\text{N}}{\text{m}^2} \right)$
G	=	αE_D	
h	=	film thickness	in (m)
h_o	=	inlet film thickness at $x = -b$	in (m)
h^*	=	reference film thickness at $\frac{dp}{dx} = 0$, $h^* = h_c$	in (m)
h_c	=	center film thickness at $x = 0$	in (m)
h_{\min}	=	minimum film thickness	in (m)
H	=	h / h^*	
H^*	=	h^* / R	
H_c	=	h_c / R	
k, j	=	grid point numbers for the x coordinate	
k_a	=	grid point numbers at $x = x_a$	

n_1, n_2, n_3	=	exponents used in the film thickness formula	
m	=	indices in Eq. (A-11)	
n	=	iteration number	
K	=	see Eq. (A-12, A-13, and A-14)	
K_f	=	thermal conductivity of the lubricant	$\text{lb}/\text{sec}^\circ\text{R} \left(\text{N}/\text{sec}^\circ\text{K} \right)$
p	=	pressure	
\bar{P}_{hz}	=	P_{hz}/E'	
P	=	P/P_{hz}	
q	=	$1 - \frac{1}{\mu}$	
Q	=	see Eq. (A-11)	
Q_m	=	$\frac{\mu_o (u_1 + u_2)^2}{2K_f T_o}$	
R	=	$\frac{R_1 R_2}{(R_1 + R_2)}$	
R_1, R_2	=	radius of roller 1 and 2	in (m)
S	=	$\frac{(u_1 - u_2)}{u_1}$	
T_o	=	ambient temperature of the lubricant	$^\circ\text{R} \left(^\circ\text{K} \right)$
\bar{U}	=	$\frac{\mu_o (u_1 + u_2)}{2E'R}$	
u_1, u_2	=	velocity of rollers 1 and 2	$\text{in}/\text{sec} \left(\text{m}/\text{sec} \right)$
x	=	coordinate along the film	in (m)
x^*	=	reference coordinate at $\frac{dp}{dx} = 0$	in (m)

x_a	=	coordinate separating the inlet region into two subregions	in (m)
x_b	=	coordinate separating the outlet region into two subregions	in (m)
\bar{x}	=	x/b	
x_f	=	coordinate at the termination of the film	in (m)
$\bar{\alpha}$	=	αp_{hz}	$\text{in}^2 / \text{lb} \left(\frac{\text{m}^2}{\text{N}} \right)$
α	=	pressure-viscosity coefficient	
β	=	temperature-viscosity coefficient	$^{\circ}\text{R} (^{\circ}\text{K})$
γ	=	pressure-temperature-viscosity coefficient	$^{\circ}\text{R-in}^2 / \text{lb} \left(\frac{^{\circ}\text{K-m}^2}{\text{N}} \right)$
μ	=	viscosity of the lubricant	$\text{lb-sec} / \text{in}^2 \left(\text{N-sec} / \text{in}^2 \right)$
μ_o	=	inlet viscosity	$\text{lb-sec} / \text{in}^2 \left(\text{N-sec} / \text{in}^2 \right)$
$\bar{\mu}$	=	μ / μ_o	
ρ	=	density of the lubricant	$\text{lb} / \text{in}^3 \left(\text{N} / \text{m}^3 \right)$
ρ^*	=	density at $x - x^*$	$\text{lb} / \text{in}^3 \left(\text{N} / \text{m}^3 \right)$
$\bar{\rho}$	=	ρ / ρ_o	
ρ_o	=	ambient density	$\text{lb} / \text{in}^3 \left(\text{N} / \text{m}^3 \right)$
ν_1, ν_2	=	Poisson's ratio of rollers 1 and 2	
$\bar{\xi}$	=	dummy variable for \bar{x}	
φ_T	=	thermal reduction factor	
ψ	=	see Eq. (A-10)	

APPENDIX B

Numerical Solution for the Inlet Region

The inlet half of the contact zone, which is bounded by $-\infty < \bar{x} < 0$, is further divided into two subregions as shown in Fig. 13. The first subregion is bounded by $-\infty < \bar{x} < \bar{x}_a$, and the pressure in this region is obtained by direct integration of the Reynolds equation considering the film profile being known in each iteration.

In order to improve the accuracy in the direct integration of Reynolds equation in this region, a new dimensionless function, q , is introduced, where

$$q = 1 - \frac{1}{\bar{\mu}} \quad (A1)$$

Using this function, Eq. (4) takes the form

$$\frac{dq}{d\bar{x}} = C_5 \frac{d(\ln \bar{\mu})}{dP} \left(\frac{H - \frac{\bar{\rho}^*}{\bar{\rho}}}{H^3} \right) \quad (A2)$$

where $C_5 = 48\bar{U}/(H^*)^2$ and $h^* = h_c$ or $H^* = H_c$

Integrating (A2) gives

$$q(\bar{x}) = C_5 \int_{-\infty}^{\bar{x}} \frac{d(\ln \bar{\mu})}{dP} \left(\frac{H - \frac{\bar{\rho}^*}{\bar{\rho}}}{H^3} \right) d\bar{\xi} \quad (A3)$$

The pressure is then obtained by solving numerically the following implicit equation using Newton's method.

$$\bar{\mu}(P) = \frac{1}{1 - q(\bar{x})} \quad (A4)$$

It was found that this procedure gives a much improved convergence of the pressure profile in the first subregion at the inlet.

For viscosity varying exponentially with the pressure

$$\bar{\mu} = e^{\bar{\alpha}P} \quad (\text{A5})$$

$$\frac{d(\ln \bar{\mu})}{dP} = \bar{\alpha} \quad (\text{A6})$$

$$q = 1 - e^{-\bar{\alpha}P} \quad (\text{A7})$$

$$P = -\frac{1}{\bar{\alpha}} \ln [1 - q(\bar{x})] \quad (\text{A8})$$

In the second subregion, the pressure and film profile are solved simultaneously by combining Eqs. (4) and (5) to form

$$\frac{H^3}{\bar{\mu}} \frac{dP}{d\bar{x}} - C_5 \left[1 + C_1 \left(\frac{\bar{x}^2}{2} - \frac{1}{\pi} \int_{-\infty}^{\bar{x}_f} P(\bar{\xi}) \ln \frac{|\bar{\xi} - \bar{x}|}{|\bar{\xi}|} d\bar{\xi} \right) - \frac{\bar{\rho}^*}{\bar{\rho}} \right] = 0 \quad (\text{A9})$$

Where $C_1 = 16\bar{P}_{hz}^2/H^*$

Written in finite difference approximation, Eq. (A9) becomes, $\Psi_k \equiv 0$, where

$$\Psi_k = \frac{(H_{k-\frac{1}{2}})^3}{\bar{\mu}_{k-\frac{1}{2}}} \frac{(P_k - P_{k-1})}{(\bar{x}_k - \bar{x}_{k-1})} - C_5 \left[1 + C_1 \left(\frac{\bar{x}_{k-\frac{1}{2}}^2}{2} - \frac{1}{\pi} \sum_{j=1,3,5,\dots}^{k_f-2} P_j Q(k-\frac{1}{2}, j) - \frac{\bar{\rho}^*}{\bar{\rho}_{k-\frac{1}{2}}} \right) \right] \quad (\text{A10})$$

Equations (A10) are a set of n equations for $k = k_a + 1$ to k_o , and

$n = k_o - k_a$. The $Q(k-\frac{1}{2}, j)$ are the quadrature formulae for the singular logarithmic kernel given in [22].

$$Q(k-\frac{1}{2}, j) = \frac{1}{2} \sum_{m=1}^3 \left[K_m(k, j) + K_m(k-1, j) - K_m(k_o, j) - K_m(k_o-1, j) \right] \quad (A11)$$

and

$$K_1(k, j_j) = \frac{1}{2\delta_j} (-3v_j - v_{j+2}) - \frac{\bar{v}_j}{3\delta_j^2} - u_j (\ln|u_j| - 1) \quad (A12)$$

$$K_2(k, j_j) = \frac{2}{\delta_j} (v_j + v_{j+2}) + \frac{2\bar{v}_j}{3\delta_j^2} \quad (A13)$$

$$K_3(k, j_j) = \frac{1}{2\delta_j} (-v_j - 3v_{j+2}) - \frac{\bar{v}_j}{3\delta_j^2} + u_{j+2} (\ln|u_{j+2}| - 1) \quad (A14)$$

where

$$\delta_j = \bar{\xi}_{j+1} - \bar{\xi}_j$$

$$u_j = \bar{\xi}_j - \bar{x}_k$$

$$v_j = \frac{u_j^2}{2} \left(\ln|u_j| - \frac{3}{2} \right)$$

$$\bar{v}_j = u_j \left[v_j - \frac{u_j^2}{6} \right] - u_{j+2} \left[v_{j+2} - \frac{u_{j+2}^2}{6} \right]$$

Similar to the procedures used in [15], Eqs. (A10) are solved by the Newton-Raphson method in the following manner for P_k .

Linearizing Eqs. (A10) and neglecting the high order terms, one obtains

$$\sum_{j=k_a}^{k_o-1} \left(\frac{\partial \Psi_k}{\partial P_j} \right)^n (\Delta P_j)^{n+1} = - (\Psi_k)^n \quad (\text{A16})$$

where the superscripts n denotes the values at nth iteration. The pressures at (n+1)th iteration are simply

$$P_j^{n+1} = P_j^n + (\Delta P_j)^{n+1} \quad (\text{A17})$$

The coefficients $\frac{\partial \Psi_k}{\partial P_j}$ take the following expressions for various values of j:

$$\frac{\partial \Psi_k}{\partial P_j} = A + B \quad (\text{A18})$$

where

$$A = \frac{C_1 C_5}{\pi} Q(k-\frac{1}{2}, j) \quad \text{for } j \neq k_a \quad (\text{A19})$$

$$A = \frac{C_1 C_5}{\pi} \sum_{\ell=1}^{k_a} \left(\frac{P_\ell}{P(k_a)} \right) Q(k-\frac{1}{2}, \ell) \quad \text{for } j = k_a \quad (\text{A20})$$

$$B = 0 \quad \text{for } j \neq k \text{ or } k-1$$

$$B = \frac{(H_{k-\frac{1}{2}})^3}{\bar{x}_k - \bar{x}_{k-1}} \left[(P_k - P_{k-1}) \left(-\frac{1}{2\bar{\mu}_{k-\frac{1}{2}}} \right) \left(\frac{\partial \ln \bar{\mu}}{\partial P} \right)_{k-\frac{1}{2}} \pm \frac{1}{\bar{\mu}_{k-\frac{1}{2}}} \right] \\ - \frac{C_5}{2} \frac{\bar{\rho}}{\bar{\rho}_{k-\frac{1}{2}}} \frac{\partial \bar{\rho}_{k-\frac{1}{2}}}{\partial P_{k-\frac{1}{2}}} \quad (\text{A21})$$

for $j = k$ the sign in front of $\frac{1}{\bar{\mu}_{k-\frac{1}{2}}}$ is plus and for $j = k-1$ the sign is minus.

The steps used in obtaining the inlet solution for a given set of H^* , \bar{P}_{hz} , G are:

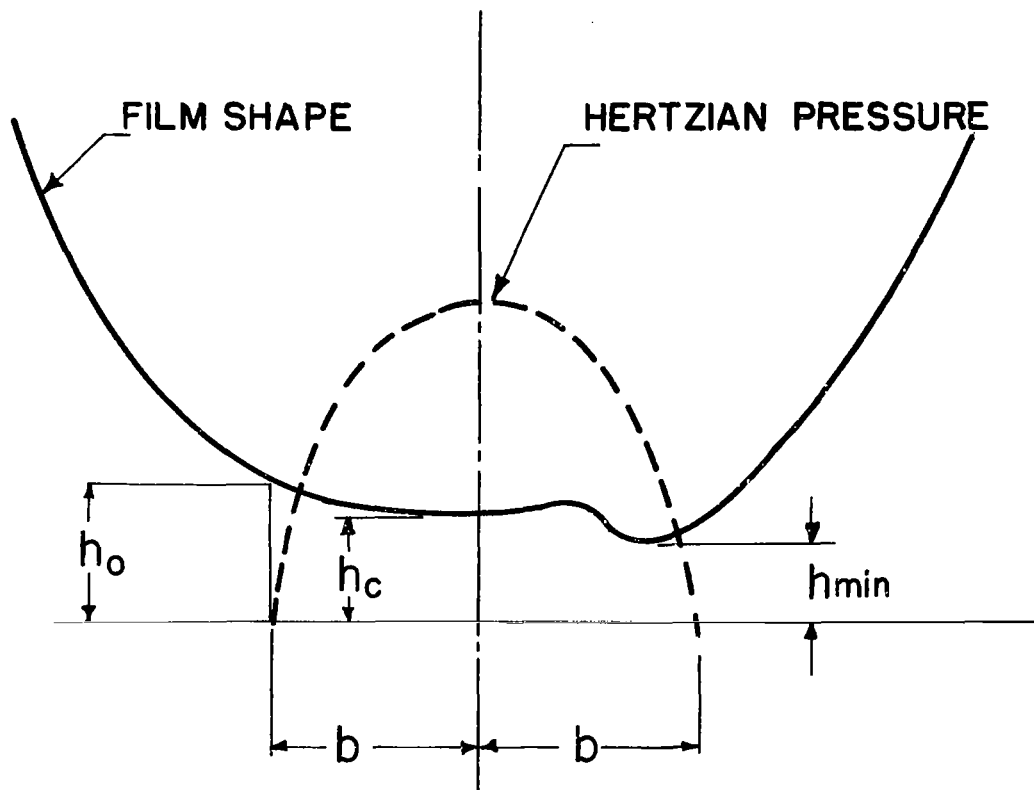
1. Assume a pressure profile for $-\infty < \bar{x} < 0$.
2. Calculate $H(\bar{x})$ for $-\infty < \bar{x} < 0$.
3. Calculate the following integral

$$I(\bar{x}) = \int_{-\infty}^{\bar{x}} \frac{d(\ln \bar{\mu})}{dp} \left(\frac{H - \bar{\rho}^* / \bar{\rho}}{H^3} \right) d\bar{\xi}$$

for $-\infty < \bar{x} \leq \bar{x}_a$.

4. Calculate $\bar{U} = \frac{(H^*)^2}{48} \frac{q(\bar{x}_a)}{I(\bar{x}_a)}$
5. Solve Eqs. (A-16) and (A-17) using Newton-Raphson method.
6. Check convergence for pressure. If not, repeat calculations starting from Step No. 2.
7. The converged solutions are represented by

\bar{U} , $P(\bar{x})$, and $H(\bar{x})$.



h_o - NOMINAL FILM

h_c - CENTRAL FILM

h_{min} - MINIMUM FILM

b - SEMI-WIDTH OF HERTZIAN CONTACT

Figure 1. - Illustration of nominal, central, and minimum film thickness.

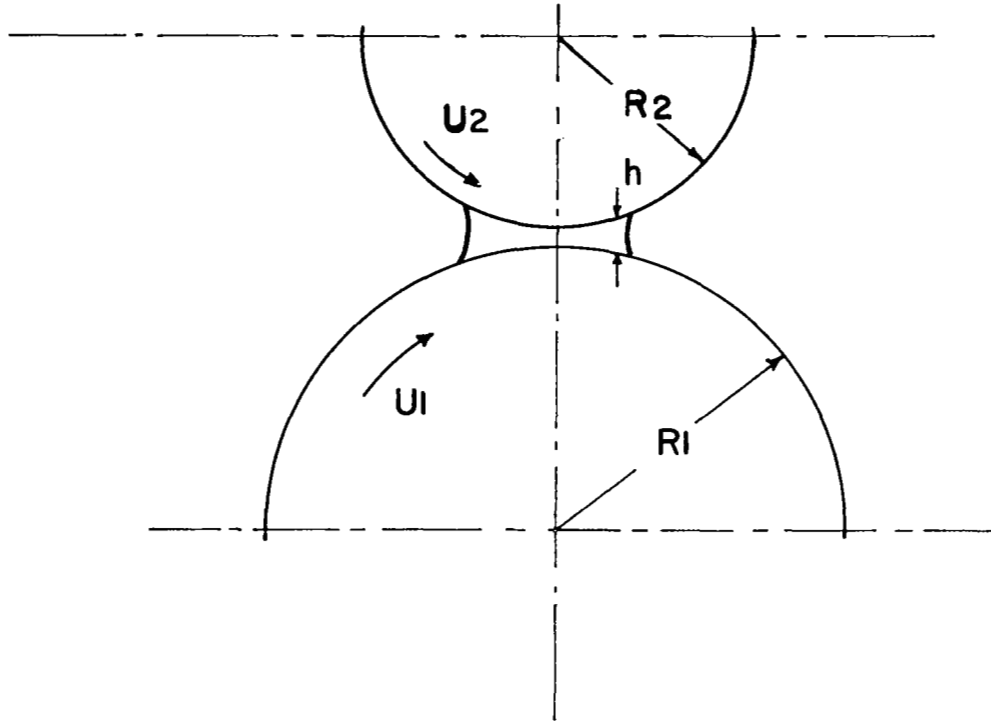


Figure 2. - Geometry of lubricated rollers.

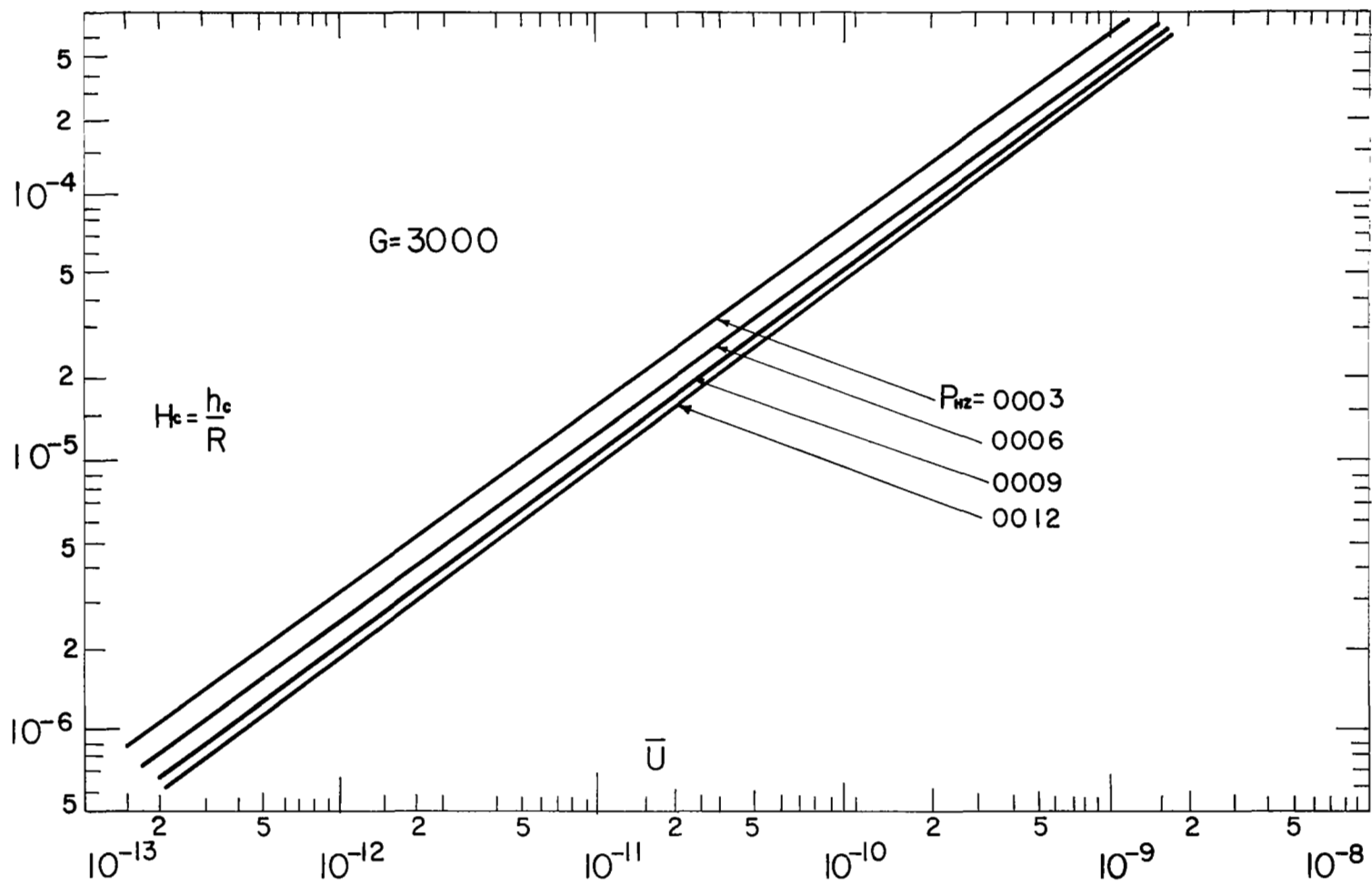


Figure 3(a). - Variation of central film thickness with rolling speed, for $G = 3000$.

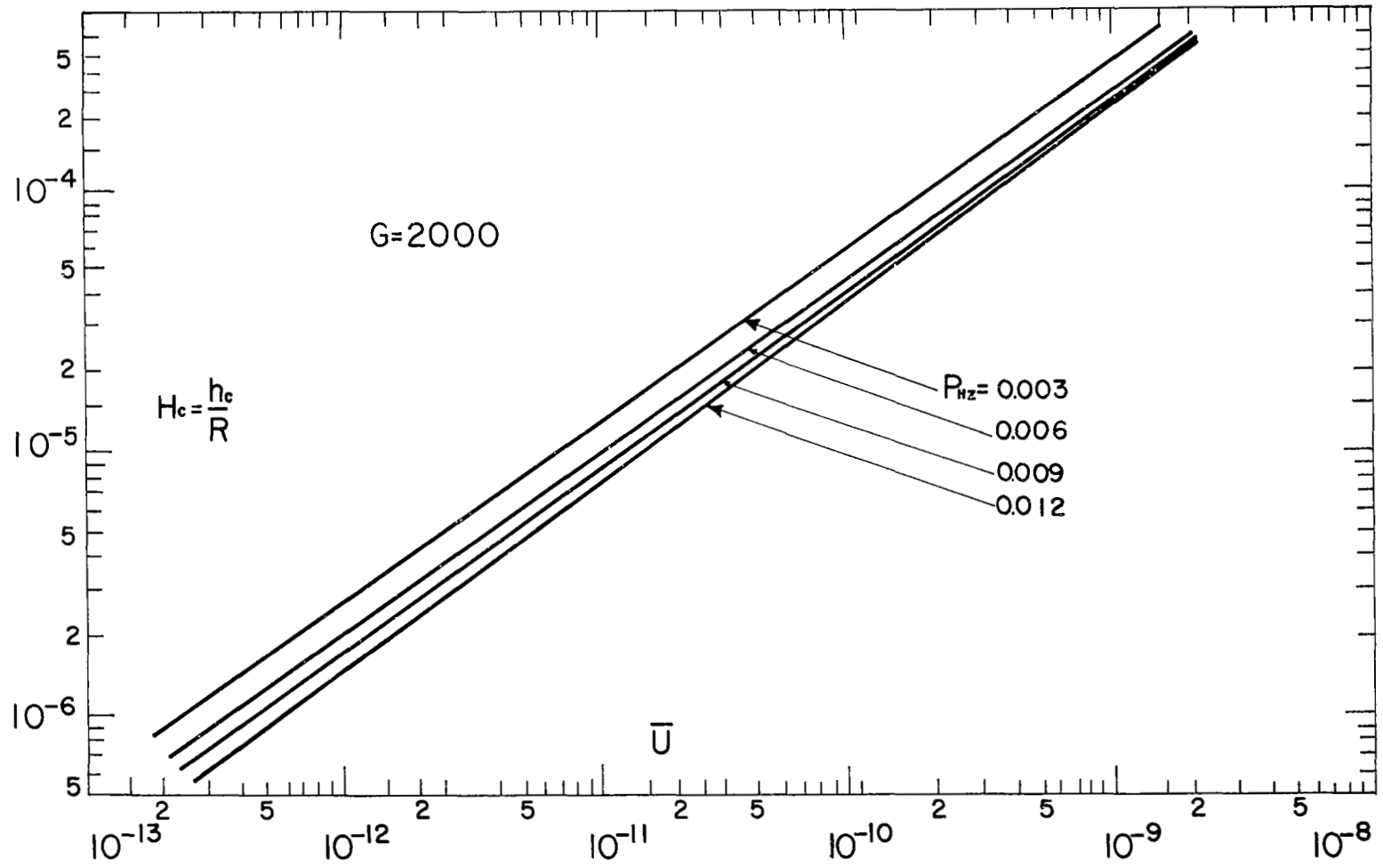


Figure 3(b). - Variation of central film thickness with rolling speed, for $G = 2000$.

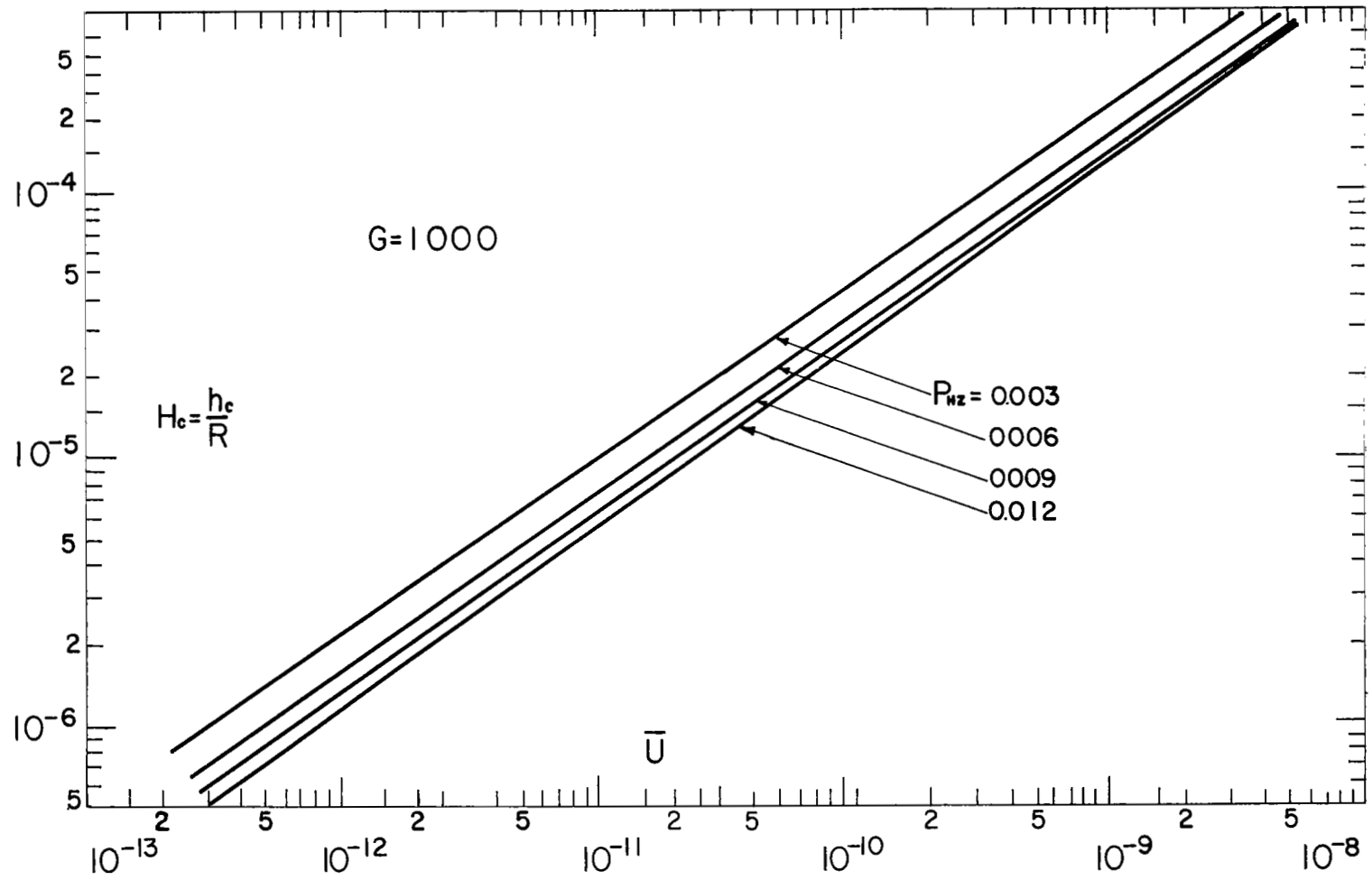


Figure 3(c). - Variation of central film thickness with rolling speed, for $G = 1000$.

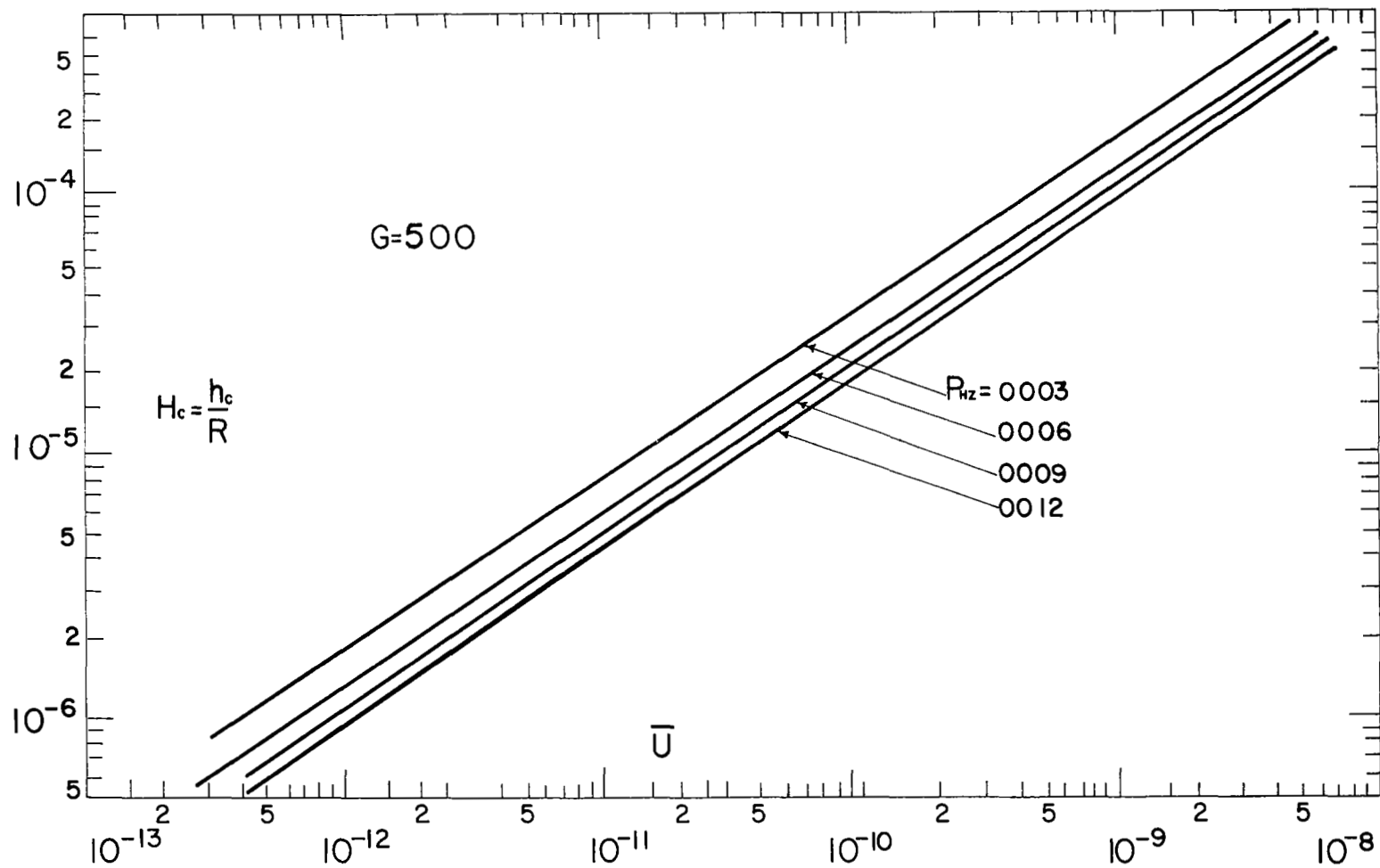


Figure 3(d). - Variation of central film thickness with rolling speed, for $G = 500$.

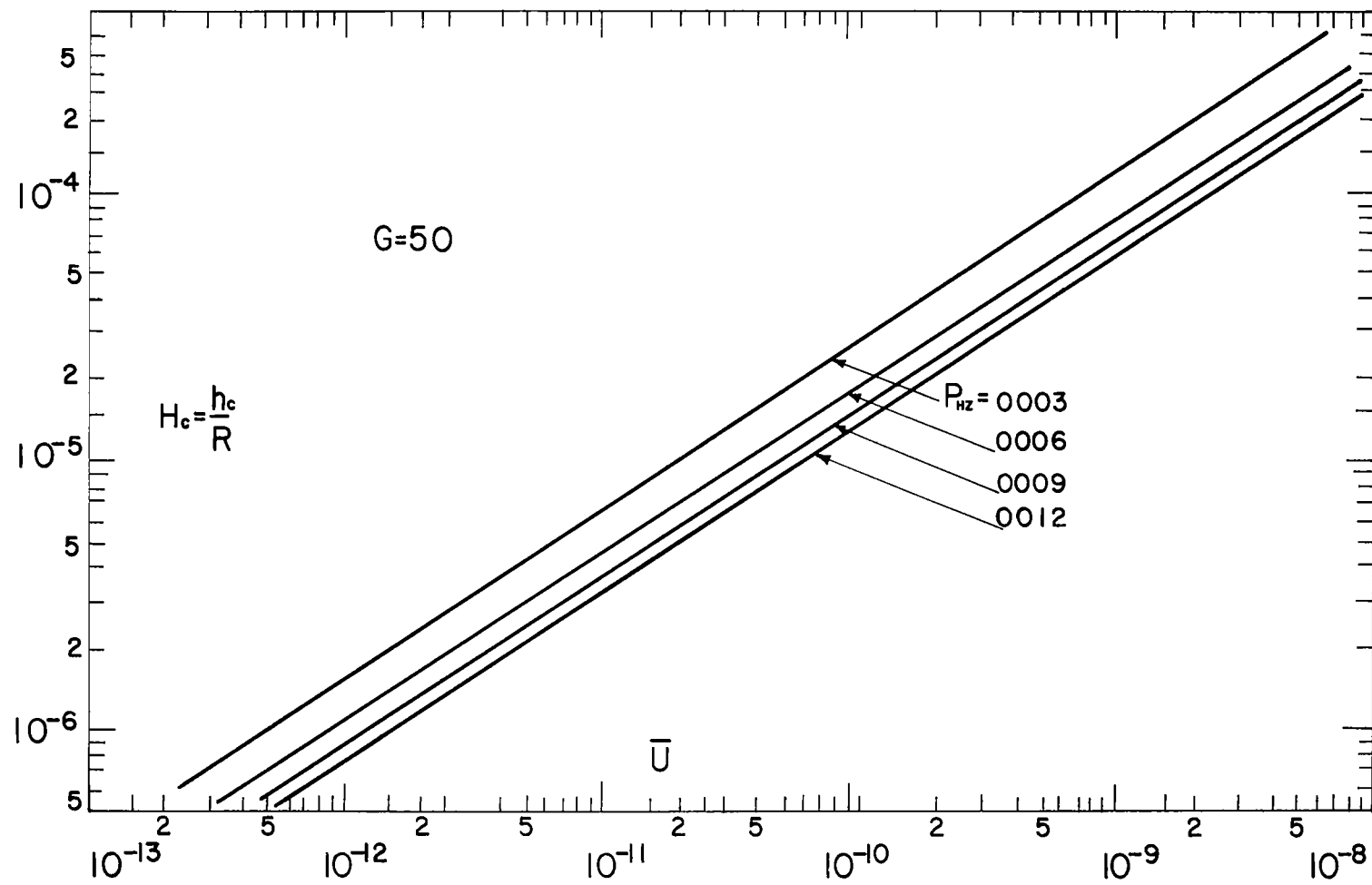


Figure 3(e). - Variation of central film thickness with rolling speed, for $G = 50$.

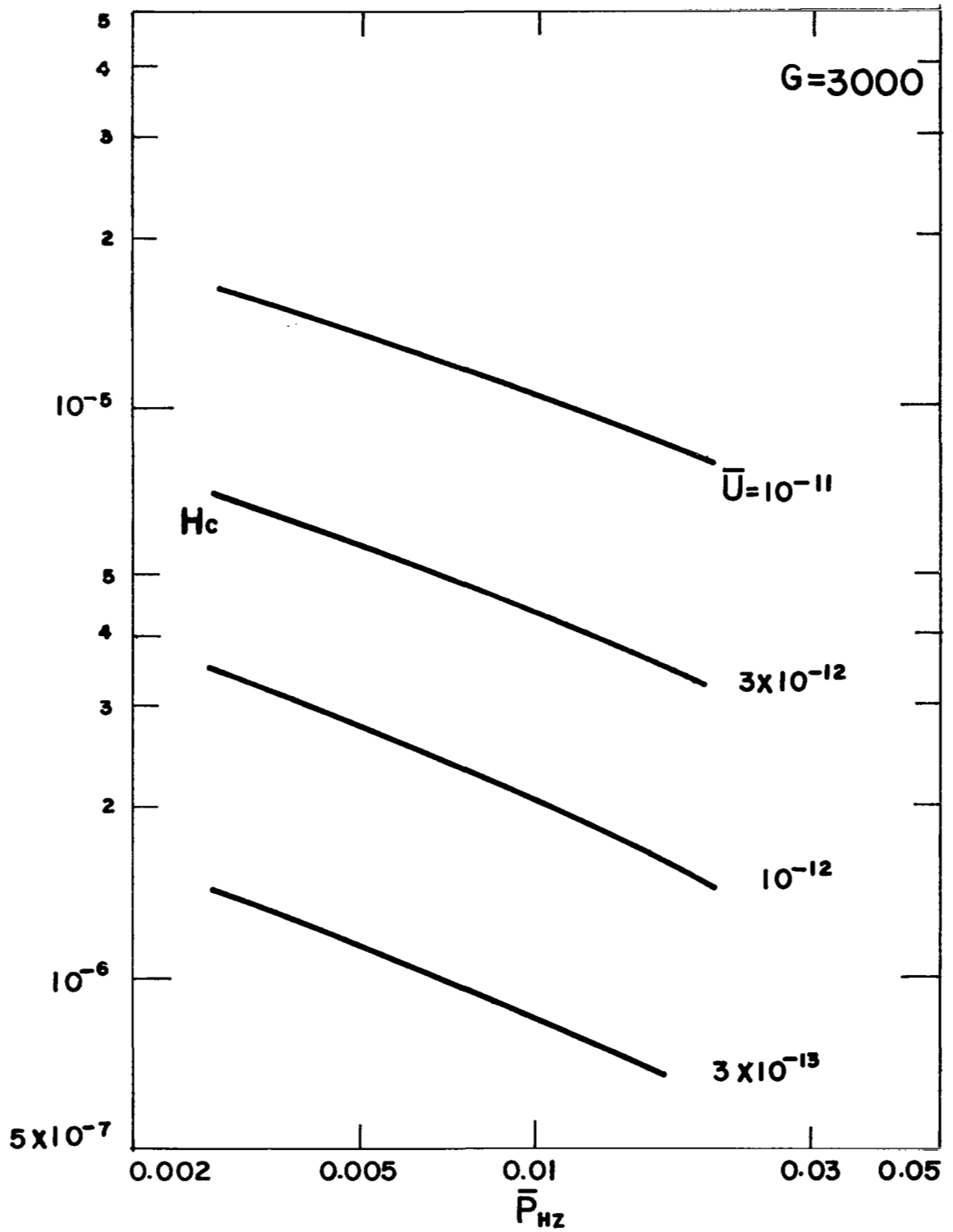


Figure 4(a). - Effect of load on central film thickness, for $G = 3000$.

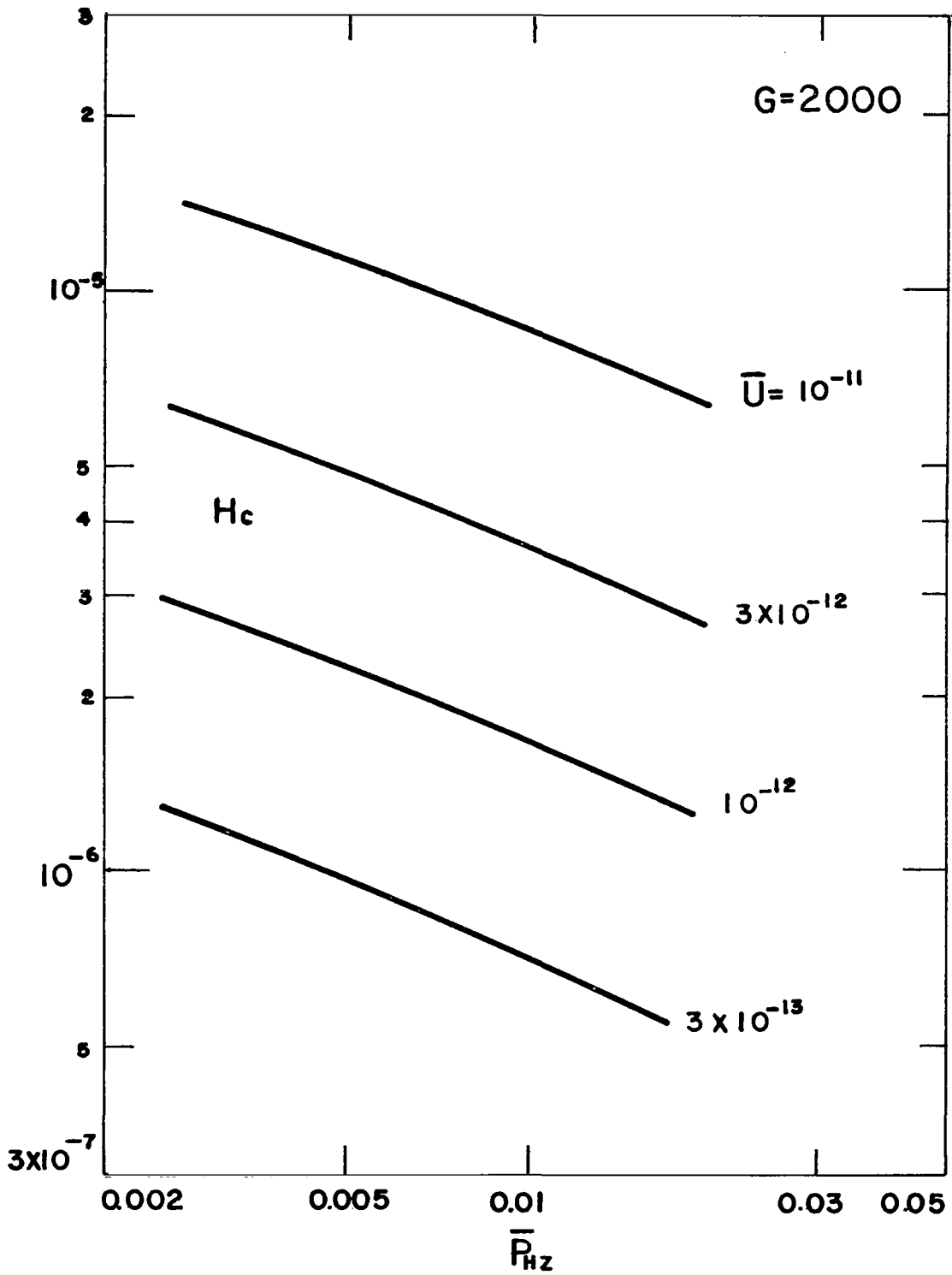


Figure 4(b). - Effect of load on central film thickness, for $G = 2000$.

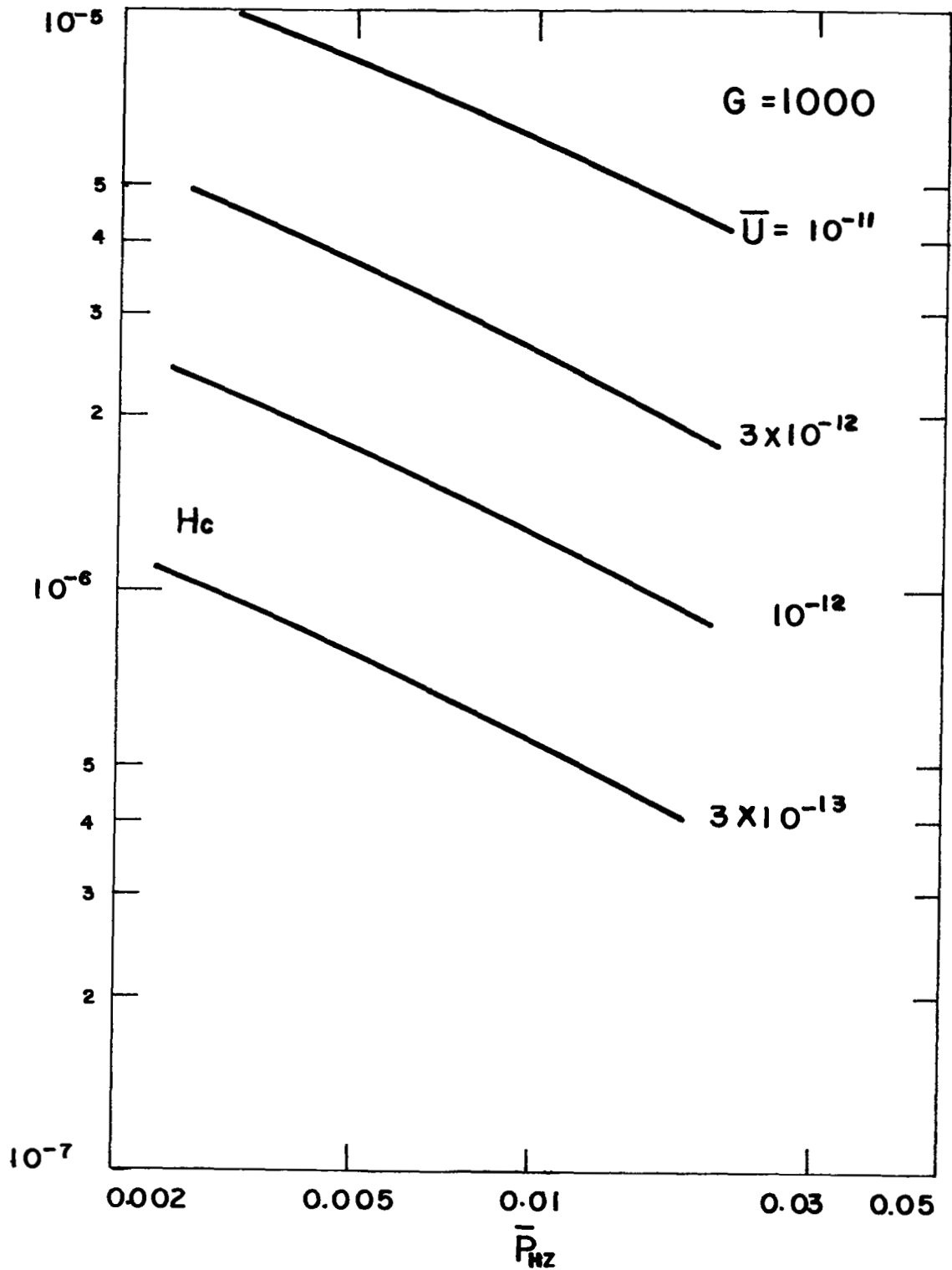


Figure 4(c). - Effect of load on central film thickness, for $G = 1000$.

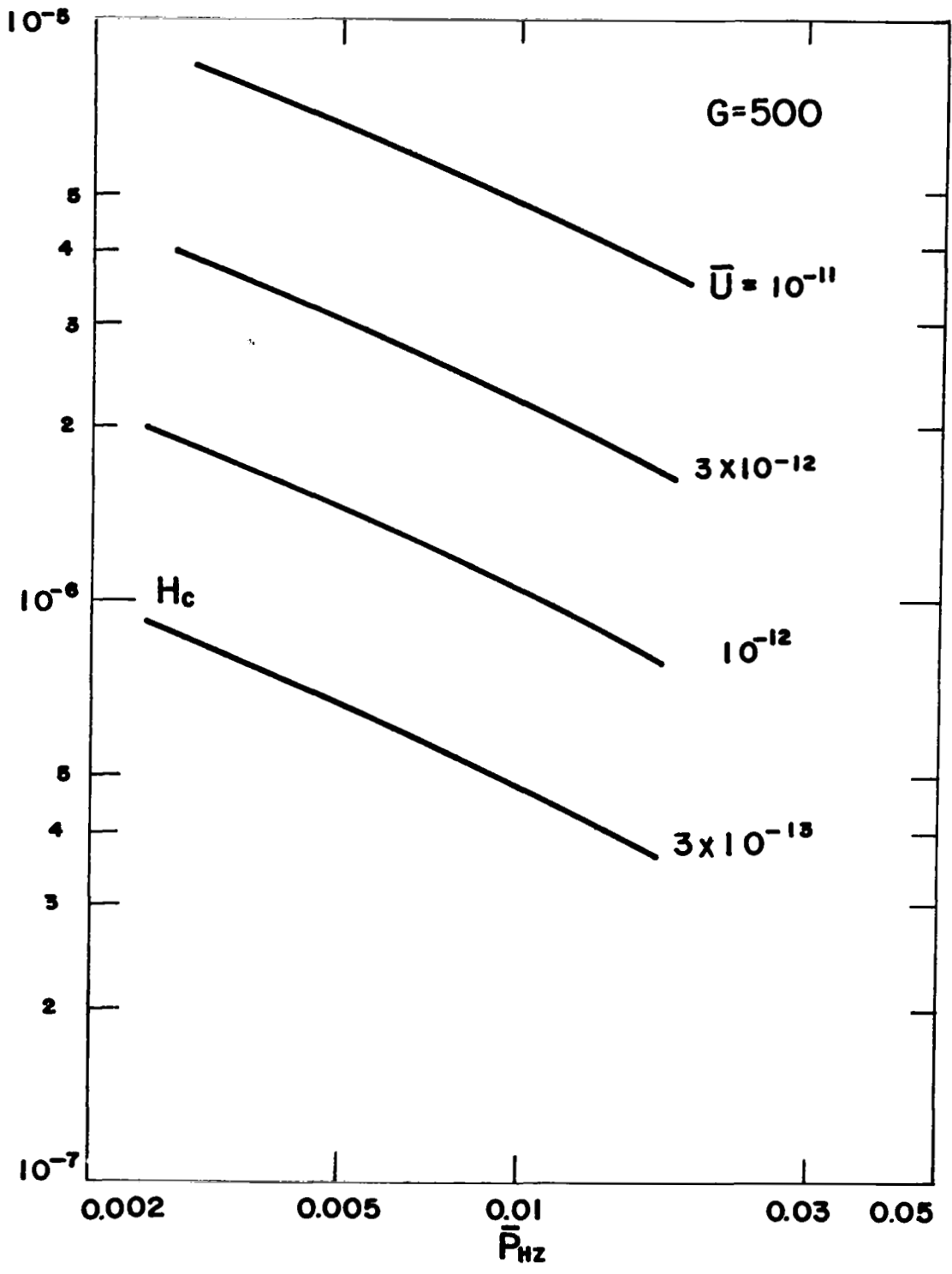


Figure 4(d). - Effect of load on central film thickness, for $G = 500$.

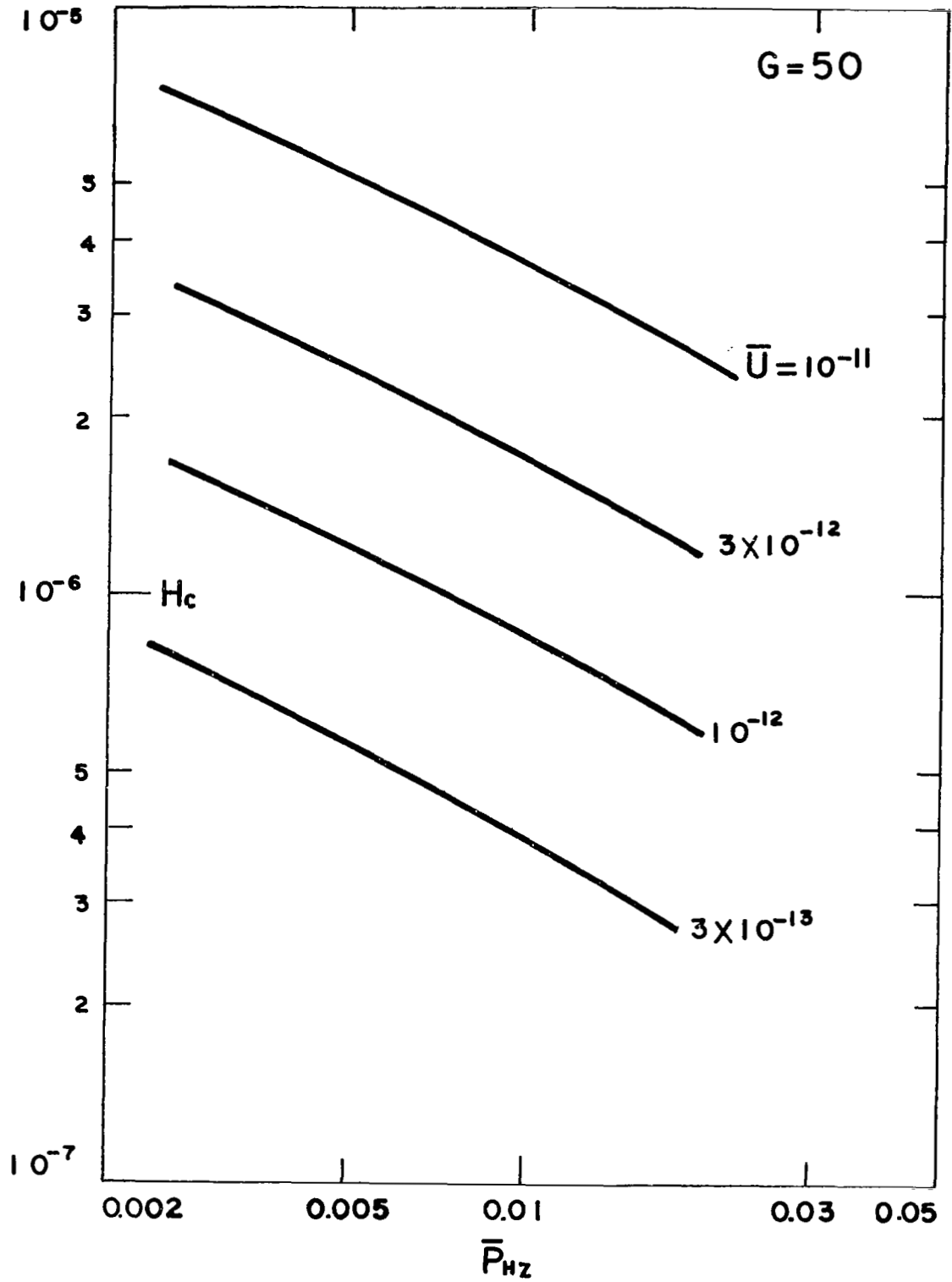


Figure 4(e). - Effect of load on central film thickness, for $G = 50$.

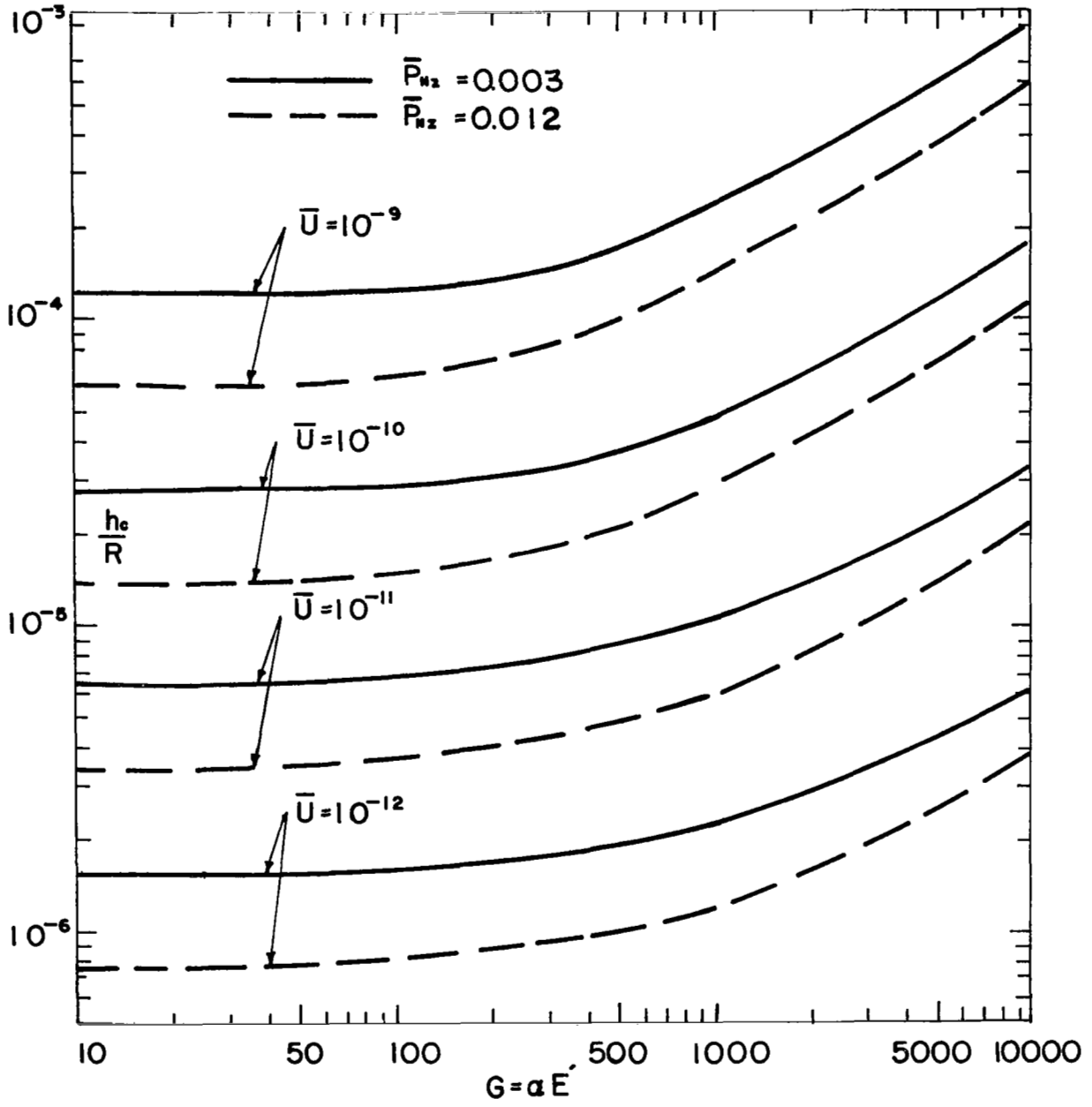


Figure 5. - Effect of pressure-viscosity coefficient on central film thickness.

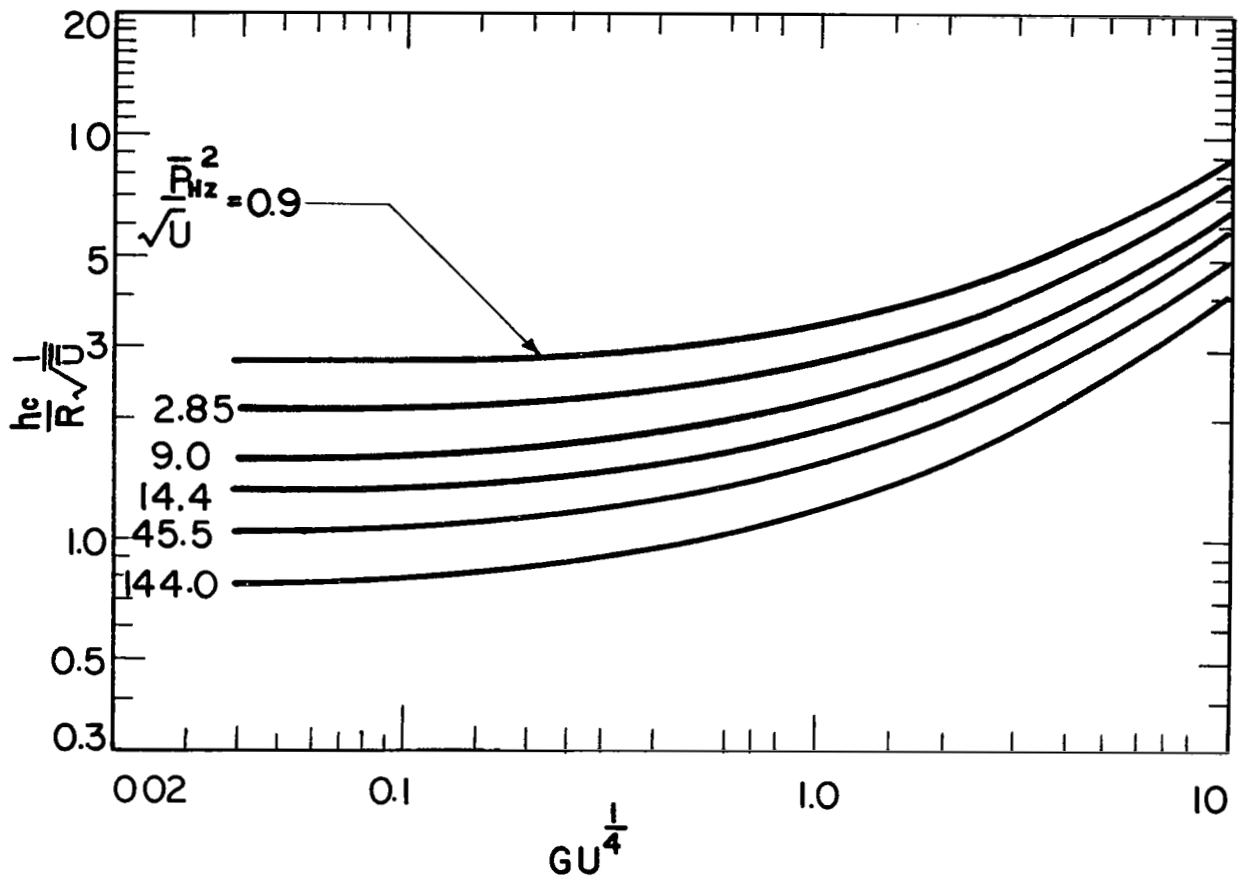


Figure 6. - Isothermal EHD results using dimensionless parameters by Moes [17].

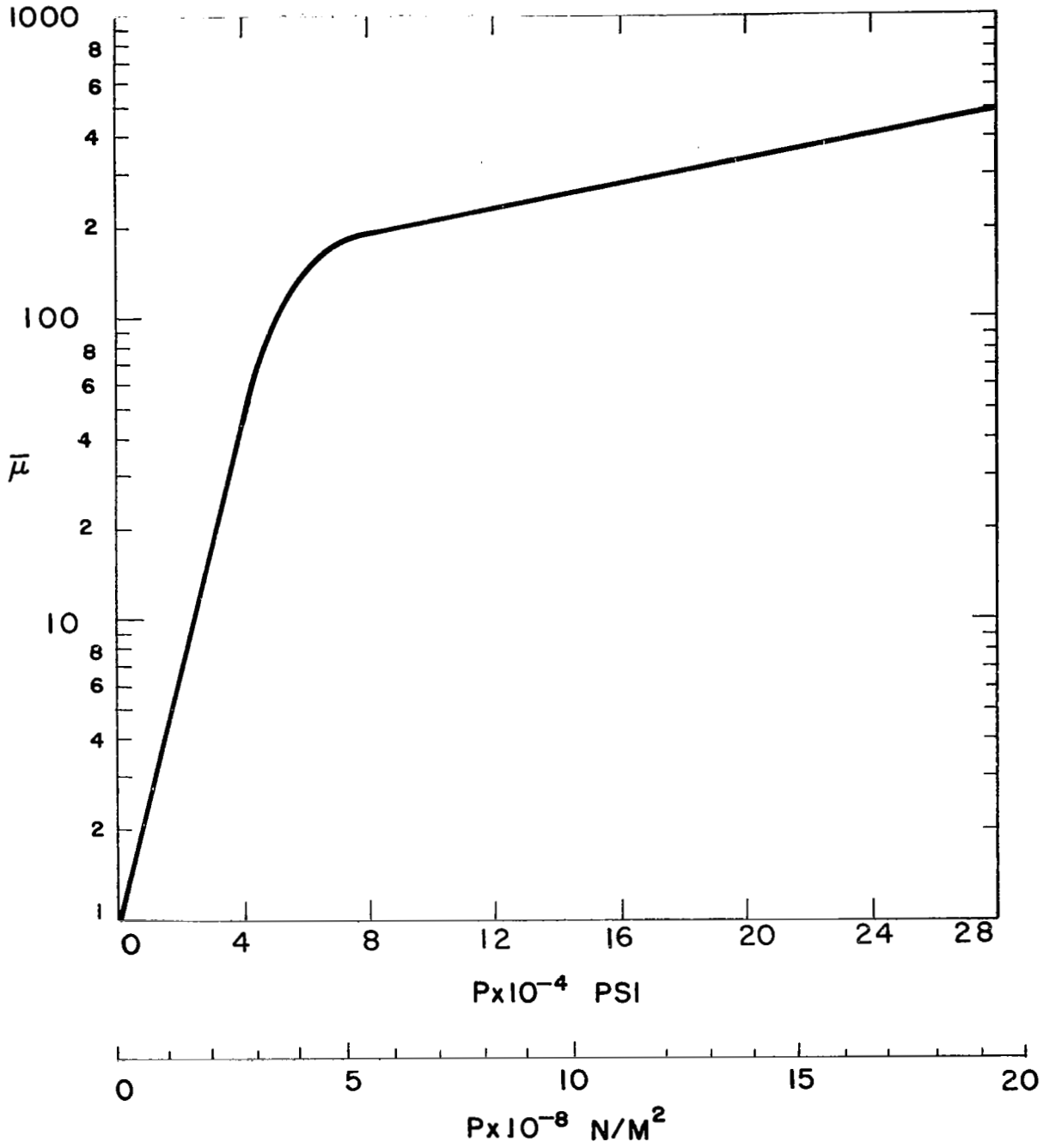


Figure 7. - Variation of viscosity with pressure for a composite exponential model.

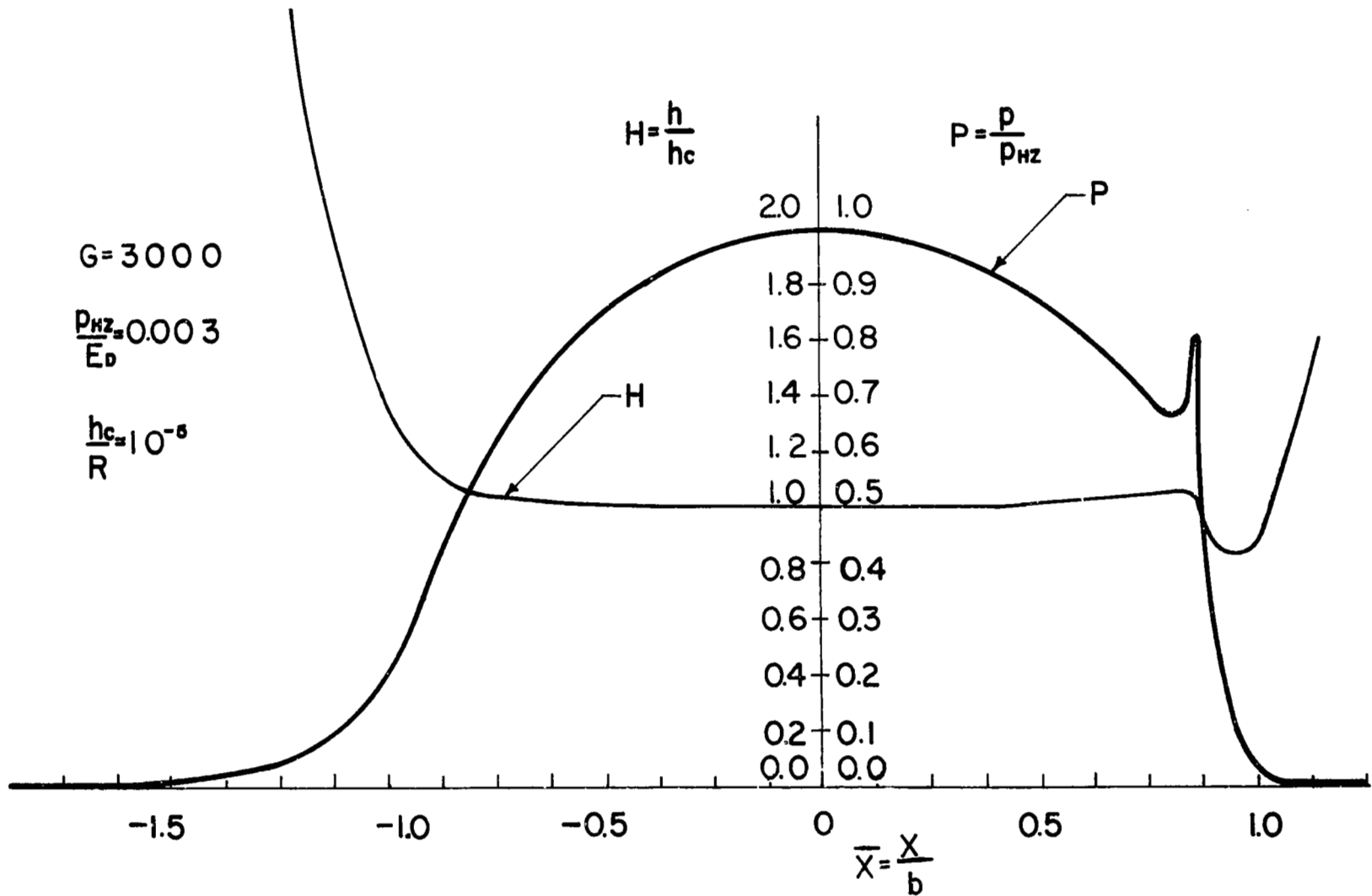


Figure 8. - Typical pressure and film thickness profiles in the entire contact region.

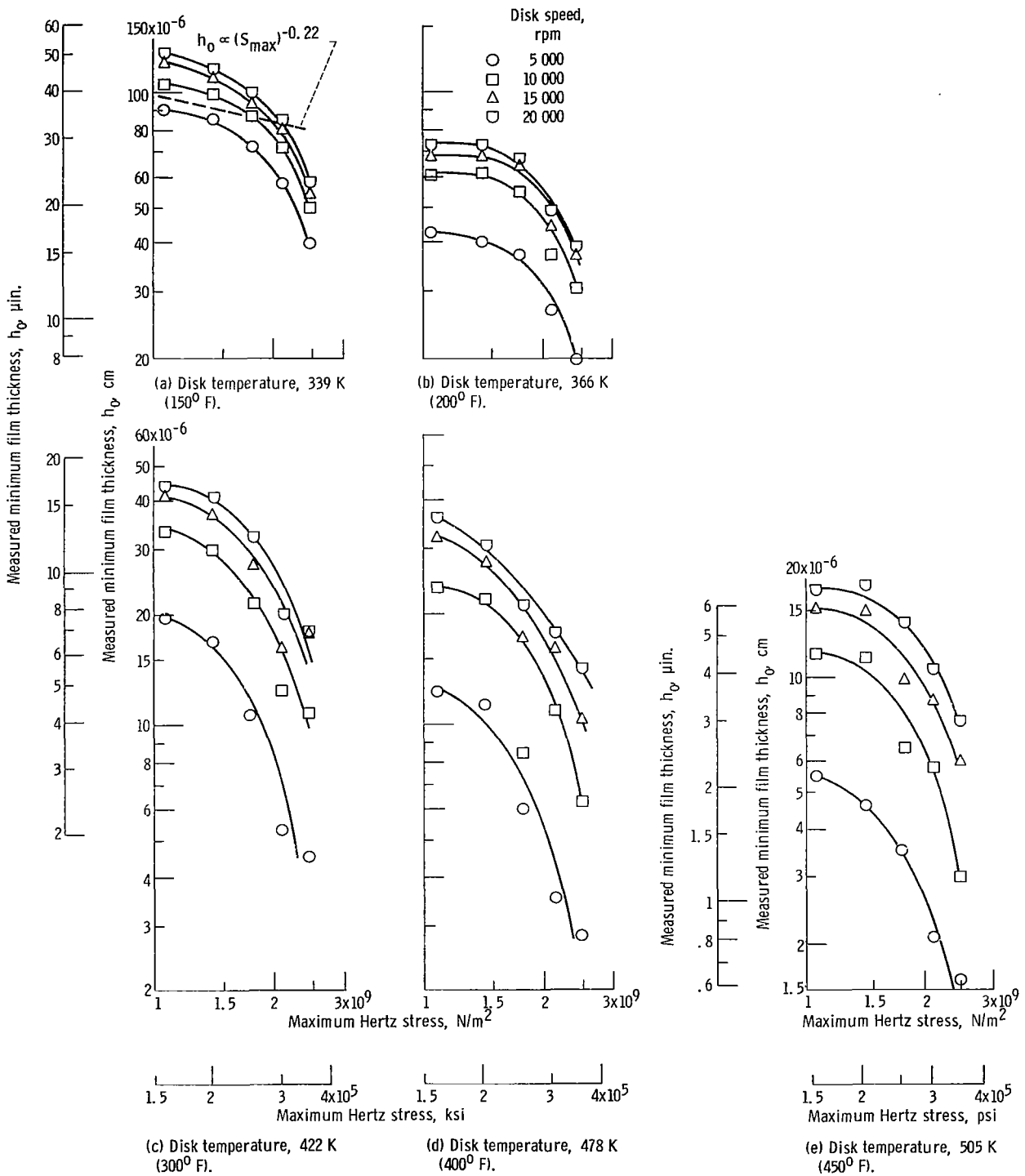


Figure 9. - Effect of maximum Hertz stress on measured minimum film thickness. Crowned-cone disks; synthetic paraffinic oil.

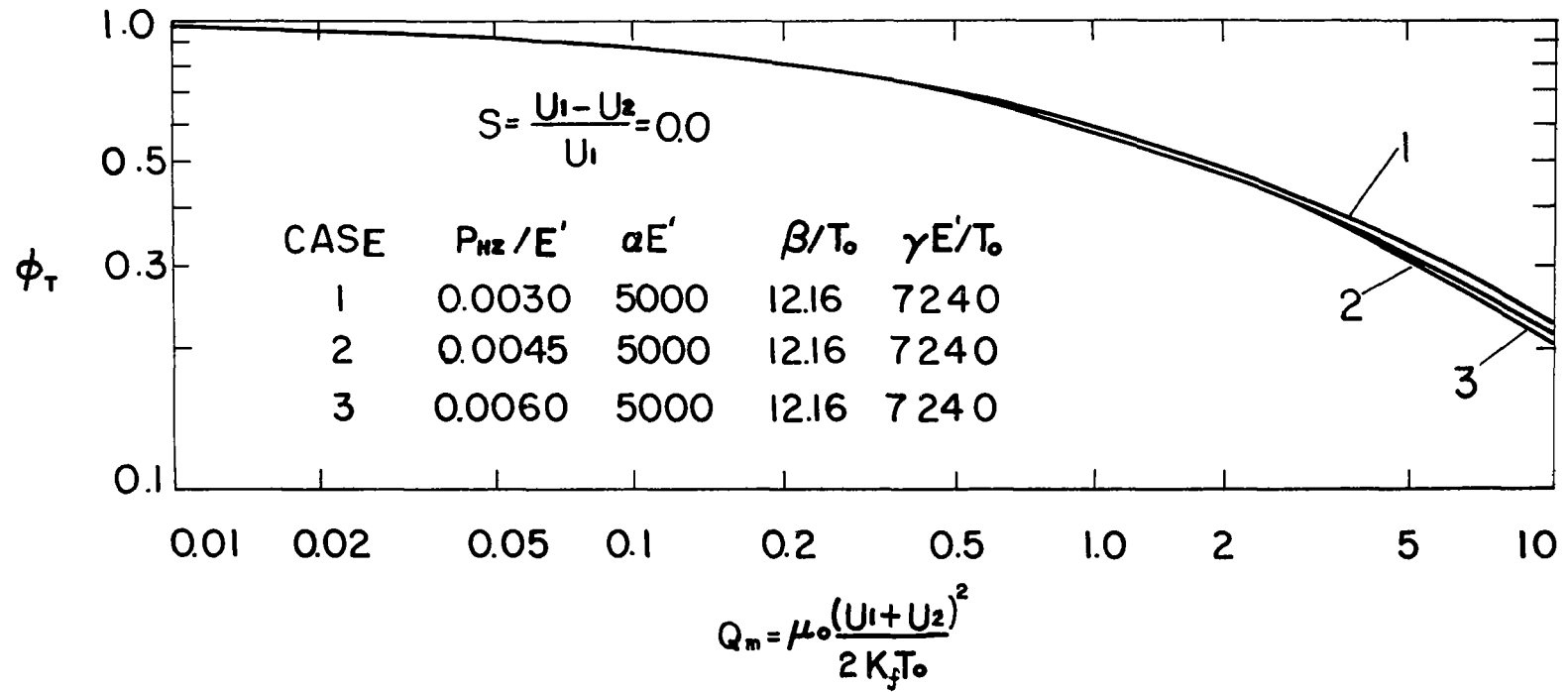


Figure 10. - Typical variation of thermal reduction factor, ϕ_T .

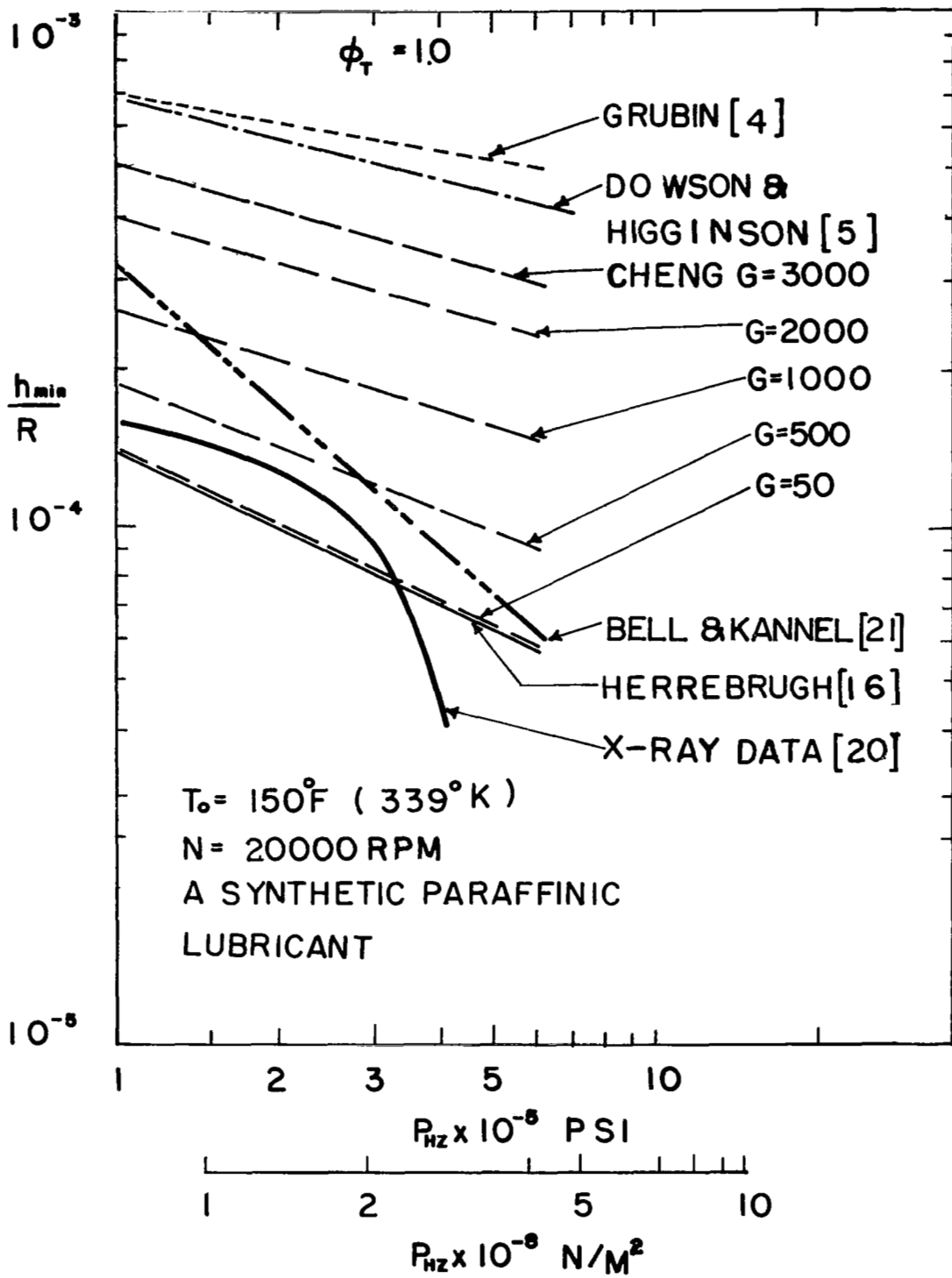


Figure 11(a). - Comparison of X-ray measured film with isothermal theories, $T_0 = 150^\circ\text{F}$, $N = 20,000 \text{ rpm}$.

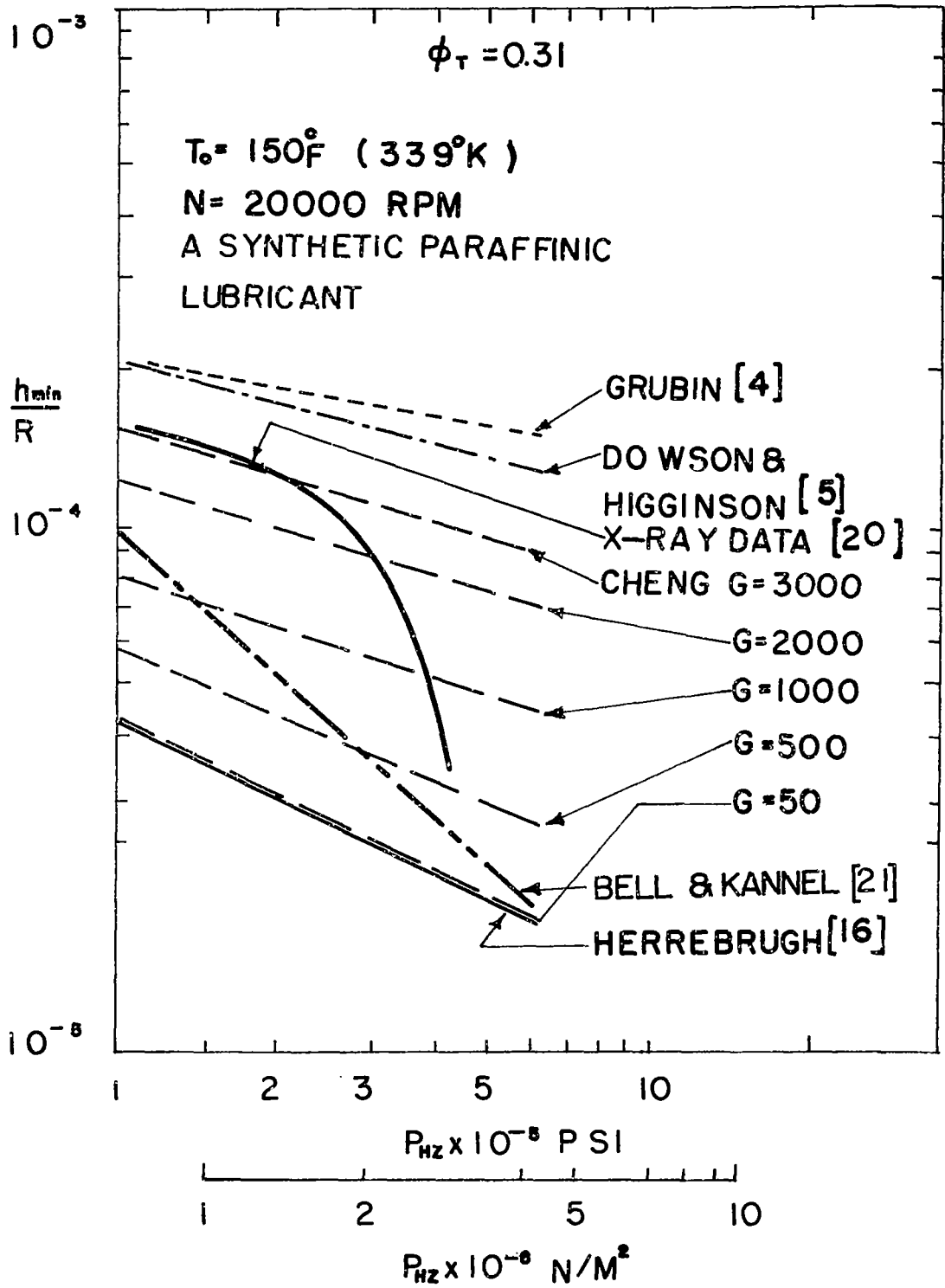


Figure 11(b). - Comparison between measured film and calculated film corrected for thermal effects, $T_0 = 150^\circ$, $N = 20,000 \text{ rpm}$.

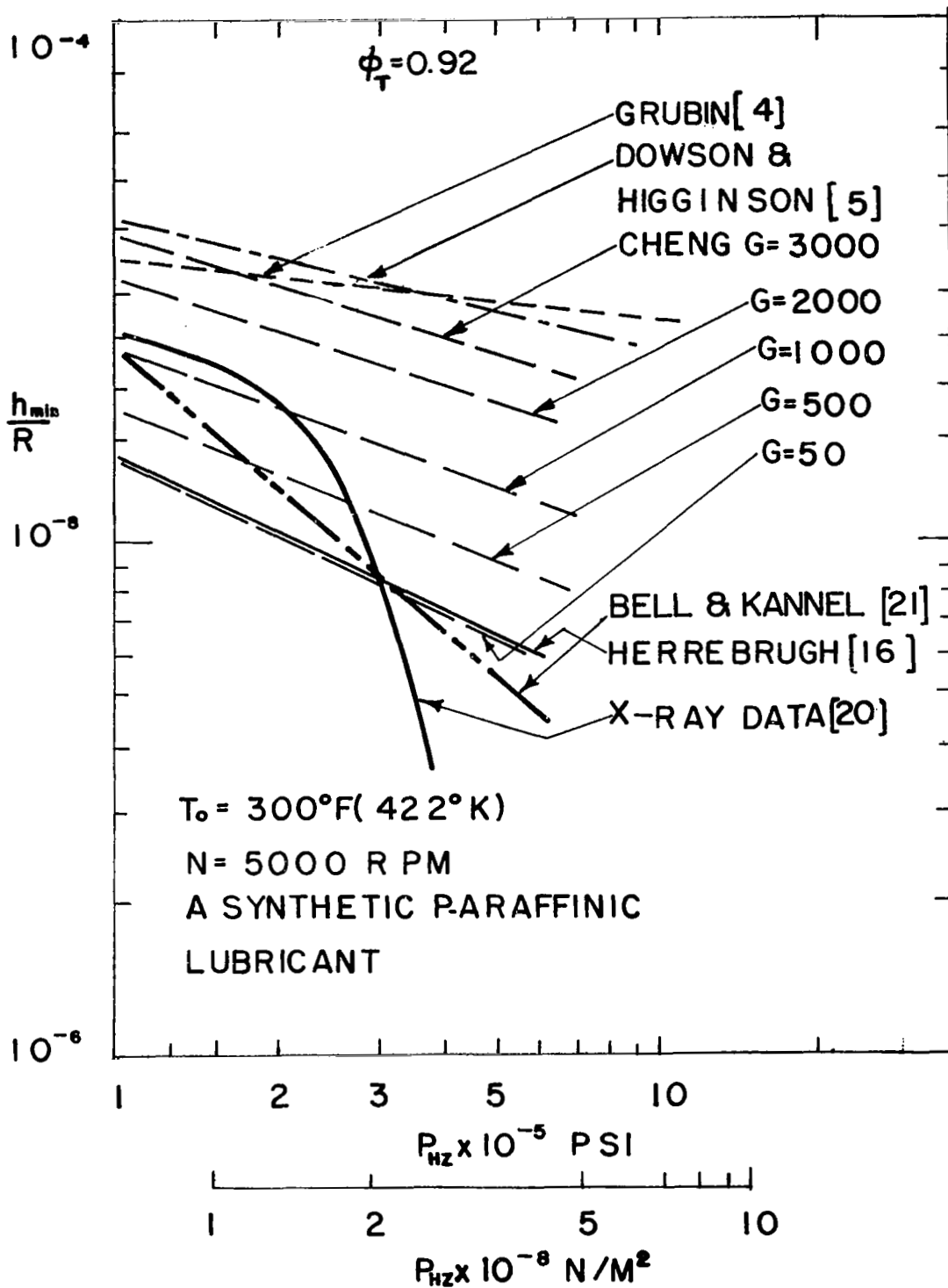


Figure 11(c). - Comparison between measured film and calculated film corrected for thermal effects, $T_0 = 300^\circ\text{F}$, $N = 20,000$ rpm.

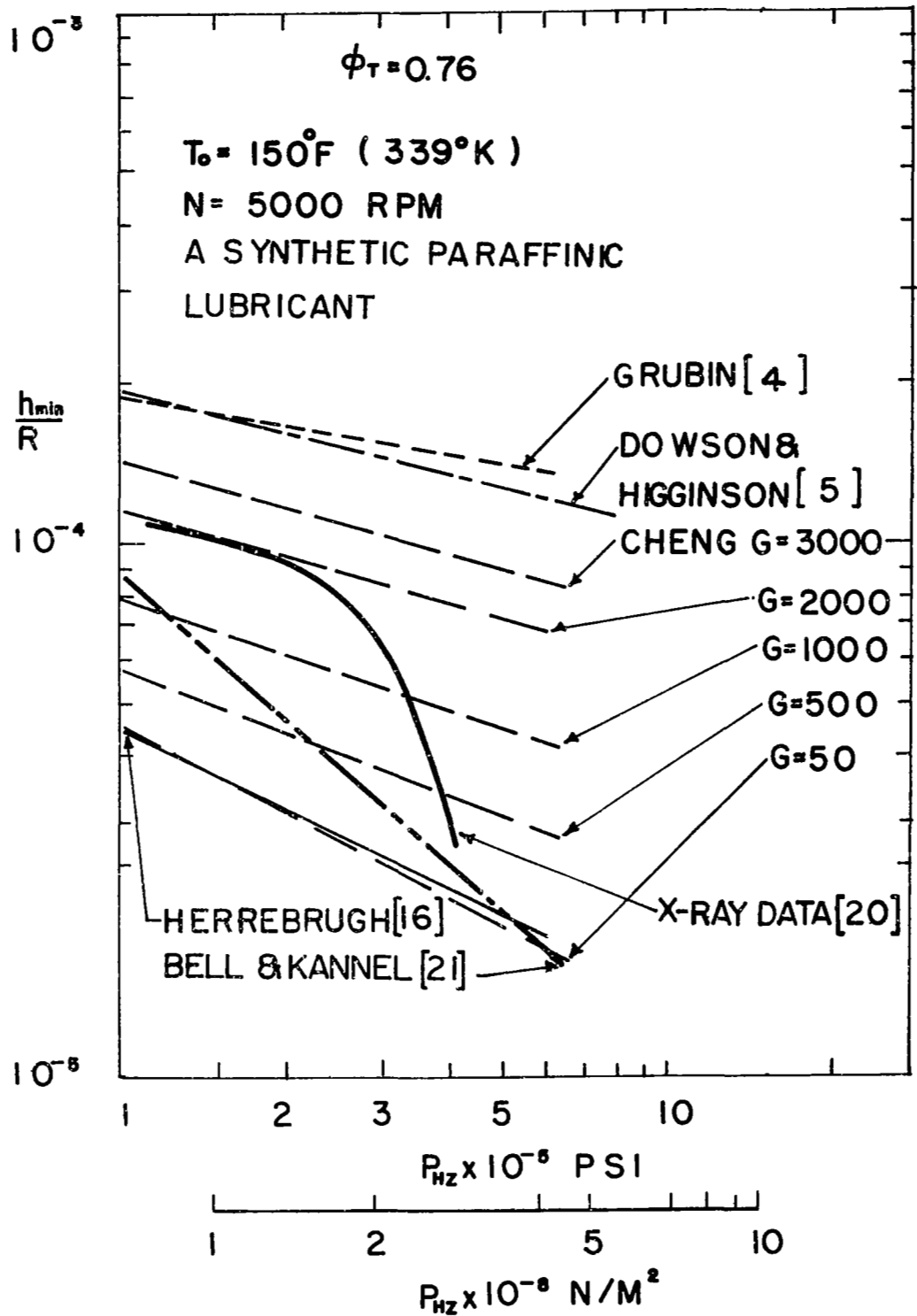


Figure 11(d). - Comparison between measured film and calculated film corrected for thermal effects, $T_0 = 150^\circ\text{F}$, $N = 5000 \text{ rpm}$.

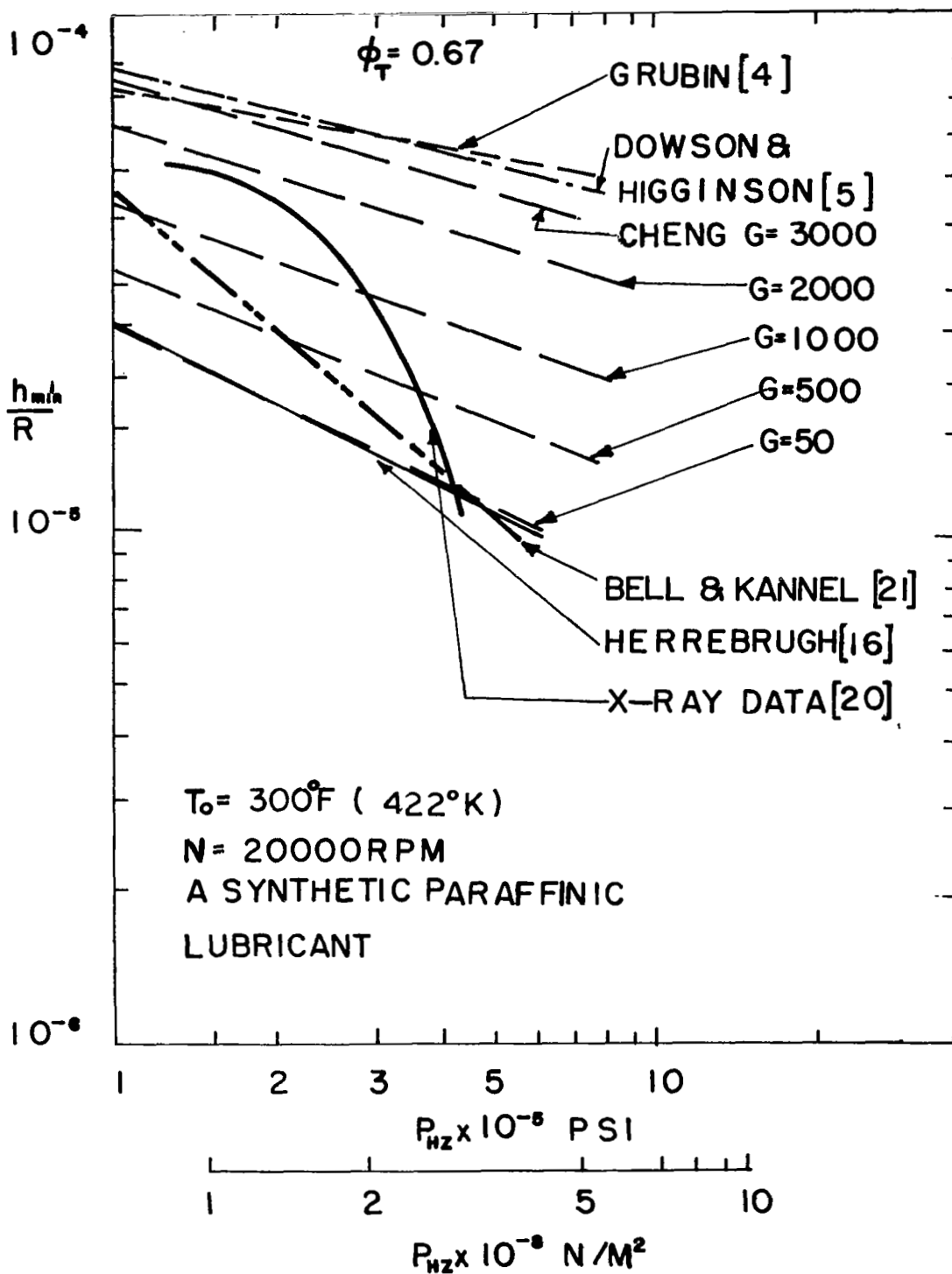


Figure 11(e). - Comparison between measured film and calculated film corrected for thermal effects, $T_0 = 300^\circ\text{F}$, $N = 5000\text{ rpm}$.

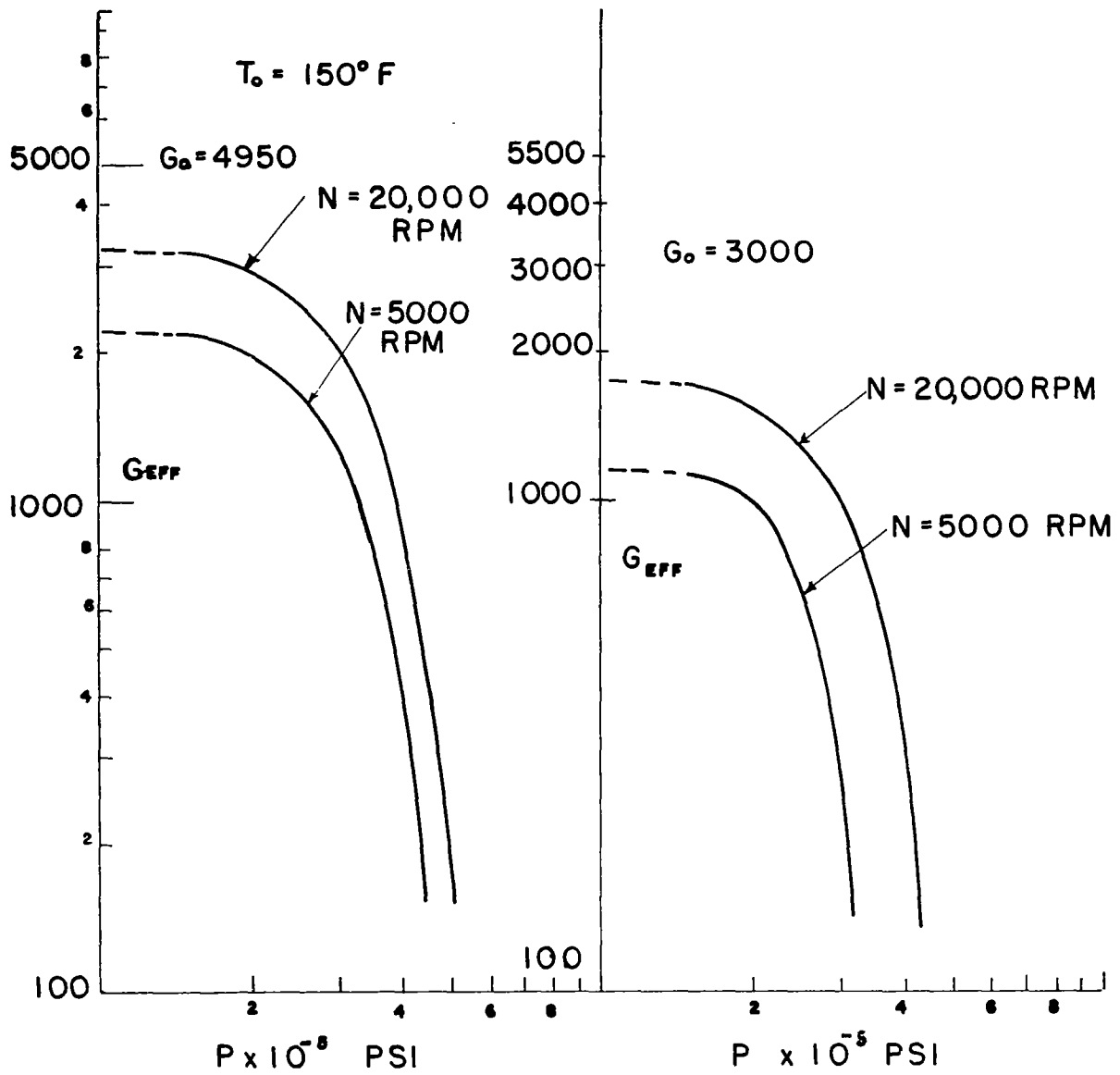


Figure 12. - Reduction of the effective pressure-viscosity parameter at high loads.

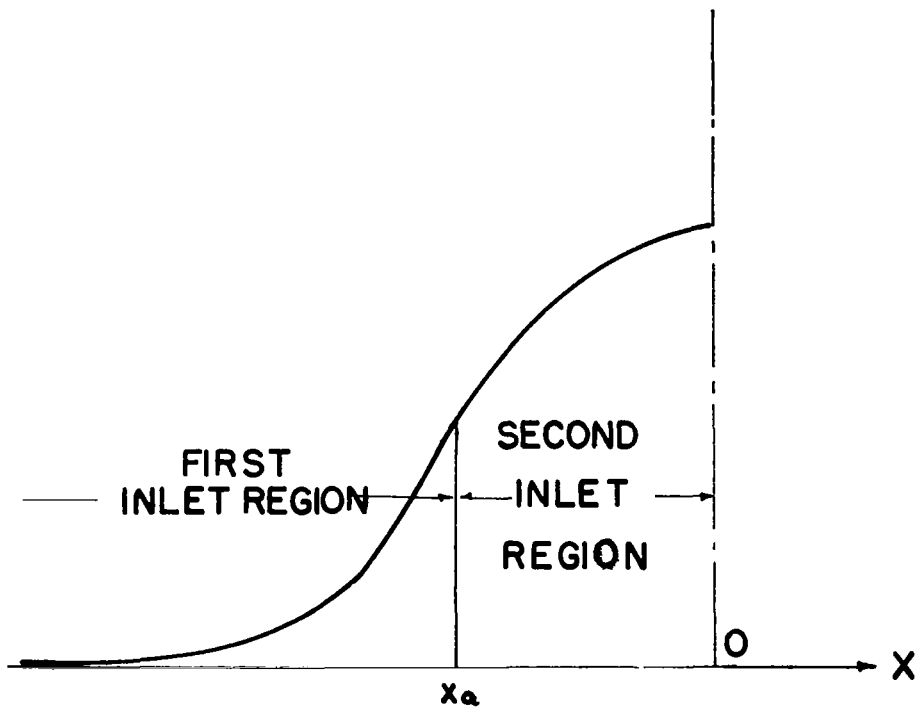


Figure 13. - Division of the inlet region.